PULSE ELECTRODEPOSITION OF Cu-Ni MULTILAYERS FROM A SINGLE BATH

By

Debabrata Pradhan

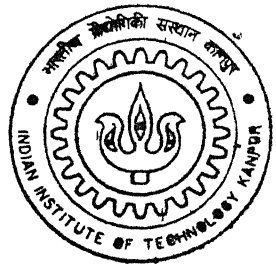

DEPARTMENT OF MATERIALS AND METALLURGICAL ENGINEERING

Indian Institute of Technology Kanpur

July, 2002

PULSE ELECTRODEPOSITION OF Cu-Ni MULTILAYERS FROM A SINGLE BATH

A Thesis submitted
in Partial Fulfillment of the Requirements
for the degree of

MASTER OF TECHNOLOGY

By

DEBABRATA PRADHAN

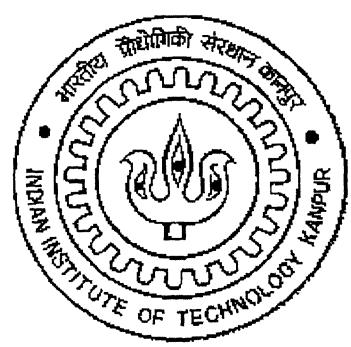

DEPARTMENT OF MATERIALS AND METALLURGICAL ENGINEERING

INDIAN INSTITUTE OF TECHNOLOGY KANPUR

JULY, 2002

CERTIFICATE

This is to certify that the investigation on **"PULSE ELECTRODEPOSITION OF Cu-Ni MULTILAYERS FROM A SINGLE BATH"** has been carried out by **Mr. DEBABRATA PRADHAN** (Roll No-Y010609) under my guidance and it has not been submitted elsewhere for a degree.

(Dr. R. Shekhar)
Professor
Department of Materials and Metallurgical Engineering
Indian Institute of Technology, Kanpur

Dated: July, 2002

ACKNOWLEDGEMENTS

At the outset I would like to convey my deepest sense of gratitude to my thesis supervisor **Prof. Rajiv Shekhar** without support, inspiration, prudence, able guidance it could never have been completed.

I am very thankful to my Project Partner Mr. Nitin Chopra and Mr. Pravesh Kumar for their contribution in the experimental works carried out.

My sincere thanks also go to Mr. U. Singh for X-RD analysis, Mr. Agnihotry for SEM micrographs, Mr. R. P. Singh for EPMA micrographs.

I thank Dr. M.N. Mungole for allowing micropolishing, sample mounting.

I would like to convey my sincere thanks to Mr. G. P. Bajpai for extending all possible and sincere help through the course of study.

Finally I would like to mention those integral part of my IIT life, my friends, who have made every moment of stay here at IITK to rejoice in future. The list is endless, still, the support, cooperation and help rendered by my laboratory partners Manindra, Mr. K. Sanjay, Lenka, Priti and my batch mate Subho, Jayanta, Bikas, Tapas, Pinaki, Sagnik, Amlan, Arnab, can never be forgot.

Debabrata Pradhan

Date: 24th July, 2002

dedicated to my parents...

TABLE OF CONTENTS

PAGE

Abstract

Electroplating is a common long–standing industrial technique for the mass production of functional coatings in industry Recent interests in and need for coatings and materials having unique properties have initiated a renewed interest in the so called advanced electroplating. The present study of advanced electroplating is focused on the recently developed compositionally modulated materials (CMM) with giant magneto-resistance (GMR). Giant Magnetoresistance effect in nanoscale alternating magnetic/nonmagnetic metallic multilayers has evinced tremendous interest worldwide. GMR sensors have potential applications in anti-skid brakes in cars and trucks, detection of land mines, electronic surveillance of international borders and missile guidance systems. GMR materials are also extremely useful for ultra-high-density data storage in hard disk (RAM) of computers.

Electrodeposition can also be used for producing magnetic multilayers Production of multilayers by electrodeposition has a number of advantages over vacuum techniques such as low cost process, simple equipment, higher (5 μm/min) deposition rate, precise deposition control and highly reproducible, low interdiffusion between sub-layers due to lower deposition temperature and complicated geometries can be coated.

The objective of the present work was to electrodeposit Cu-Ni multilayers. Electrodeposition was carried out to optimize pulse parameters (applied voltage, frequency, duty cycle and number of cycle) for deposition of alternate layers of Cu and Ni from a single bath. Electrodeposition experiments have been done potentiostatically for the electrodeposition of Cu-Ni multilayers in nanometric scale from a single-bath sulphate electrolyte. The effect of pulse parameters and electrolyte compositions on the nature of deposit characteristics, whether it was dull/dark or bright or shining and adherent/non-adherent were determined.

After determination of the effect of pulse parameters, electrolyte composition and pH on the quality of Cu and Ni electrodeposit, the best operating conditions were obtained:

	For Cu plating	**For Ni plating**
Voltage:	1.062V - 1.498V	2.91V - 3.287V
Frequency:	1.25 Hz - 0.025 Hz	1.67 Hz - 0.069 Hz
Duty Cycle:	70 % - 90 %	33.33 % – 50 %
No. of Cycle:	3 – 60	5 – 35
H_3BO_3 Conc.:	30 g/l – 45 g/l	30 g/l – 45 g/l
pH:	2.10 – 2.90	2.10 – 2.90

LIST OF FIGURES

LIST OF TABLES

data in Fig. 4.9 - 10 for two Cu–Ni CMM multilayers with different thicknesses.

CHAPTER I

INTRODUCTION

Introduction

Compositionally modulated multilayers (CMM) consisting of alternate layers of magnetic and non-magnetic alloys exhibit Giant Magneto-Resistance. This means that if their resistance is monitored, materials exhibiting GMR can be used to detect magnetic fields. In contrast to simple Magneto-Resistance, Giant-Magneto-Resistance Materials needs smaller field to high effect. CMMs have several applications thanks to their high magnetic field sensitivity. In the field of sensors and actuators, the magnetic features are indeed considered as part of the next generation of sensors, replacing semiconductor-sensing elements for use in cars, office-machinery and house hold appliances.

A brief idea of GMR material, their structure and applications are discussed below.

1.1. Giant Magneto-resistance Materials (GMR)

The "giant magnetoresistive" effect was discovered in the late 1980s by two European scientists working independently: Peter Grunberg [1] of the KFA research institute in Julich, Germany, and Albert Fert of the University of Paris-Sud. They saw very large resistance changes 6 percent and 50 percent, respectively in materials comprised of alternating very thin layers of various metallic elements. This discovery took the scientific community by surprise; physicists did not widely believe that such an effect was physically possible. These experiments were performed at low temperatures and in the presence of very high magnetic fields and used laboriously grown materials that cannot be mass-produced, but the magnitude of this discovery sent scientists around the world on a mission to see how they might be able to harness the power of the Giant Magnetoresistive effect.

Stuart Parkin and two groups of colleagues at IBM's Almaden Research Center, San Jose, Calif, quickly recognized its potential, both as an important new scientific

discovery in magnetic materials and one that might be used in sensors even more sensitive than MR heads

Currently, two types of GMR material in the standard sensor line, Multilayer and Sandwich material [2] In addition to these materials, different research and development companies like IBM, Kodak, Sony, Honeywell etc continues to develop materials and structures that will allow future generations of GMR sensors to meet the continued challenging customer performance requirements.

If we have an external magnetic field applied to a piece of conductor the electrical resistance of the specimen will change. This phenomenon is called Magneto-Resistance (MR)

Giant magnetoresistance (GMR) was first observed in layered Fe/Cr magnetic structures by Baibich et al. [3] and by Binasch et al. [4]. These structures have magnetized layers, separated by a nonmagnetic spacer metal. Here the layer thicknesses are of the order of a few tens of nanometers. GMR is characterized by the magnetoresistance ratio $\Delta R/R$, where ΔR is the total decrease of electrical resistance as the applied magnetic field is increased to saturation and R is measured in the state of parallel magnetization. The magnetic configuration of a material exhibiting GMR can be changed from one in which the electrical resistance is high to one in which it is considerably lower simply by varying the applied magnetic field. This means that if their resistance is monitored, materials exhibiting GMR can be used to detect magnetic fields Conventional materials such as Ni-Fe alloys exhibit resistance changes at room temperature of just a few percent in magnetic fields of a few oersteds. GMR sandwiches can achieve sensitivities to fields of perhaps as much as five times greater than conventional materials Consequently sensors using GMR sandwiches can offer better performance than earlier designs using conventional GMR materials.

1.1.1. GMR Structure

A GMR sandwich consists of a substrate followed by a periodic repetition - N times - of a thickness x of a ferromagnet and a thickness y of the spacer. Typically x and y range from a few Å to a few hundred Å, and N can be as small as 1 or as large as several

hundred Candidates for ferromagnetic materials are· Fe, Co, Ni, Ni-Fe, Fe-Co, Dy, Er, Gd, Ho and Tm Cu, Ag, Au, Mg, Sn, Ru, Re, Ta, Cr can be used as spacers.

1.1.2. GMR Effect

Successive ferromagnetic layers, separated by spacers, arrange themselves with their magnetization vectors either parallel (ferromagnetic coupling) or antiparallel (antiferromagnetic coupling) to each other. The magnetization is usually in the plane of the layers. An experimental survey of GMR for Co/Ru, Co/Cr, and Fe/Cr sputtered superlattice structures revealed that the saturation magnetoresistance oscillates with spacer layer thickness [5]

GMR could be observed in a wide variety of transition-metal magnetic multilayers In addition, the experiments showed that the magnitude of the GMR effect oscillated as the thickness of the nonferromagnetic spacer layers between the ferromagnetic layers was increased. This oscillation was shown to be caused by an oscillation in the sign of the interlayer exchange coupling between the ferromagnetic layers The coupling was shown to oscillate between antiferromagnetic and ferromagnetic coupling such that the magnetic moments of successive ferromagnetic layers were either parallel (ferromagnetic) or antiparallel (antiferromagnetic) in small magnetic fields.

Oscillatory coupling was shown to be a very general property of almost all transition-metal magnetic multilayered systems in which the nonferromagnetic layer comprises one of the *3d, 4d,* or *5d* transition metals or one of the noble metals [6]. The oscillation period was found to be just a few atomic layers, typically about 10 Å, but varying up to ~20 Å. Only those multilayers for which the interlayer coupling is antiferromagnetic display significant giant magnetoresistance effects. It is only in those systems that the relative orientation of the magnetic moments of neighboring layers is significantly altered by applying a magnetic field.

The application of a strong enough magnetic field, usually parallel to the plane of the layers changes the arrangement of the magnetization. The antiferromagnetic coupling is overcome, and the magnetic moments of all the ferromagnetic layers are forced to lie in the same direction. Simultaneously, the electrical resistance of the sample, both in the plane of the layers and perpendicular to it, decreases. This decrease can be a few percent, as in Co/Ru, or can exceed 110% [4] at room temperature as in Co/Cu multilayers. This decrease occurs for almost all configurations -- regardless of the direction of the current, the directions of the electric and magnetic fields, the chemical composition of the spacer and the structure of the interface -- as long as the magnetic arrangement changes from antiparallel to parallel upon application of the magnetic field.

1.1.3. Electronic Theory

The chief source of GMR is "spin-dependent" scattering of electrons. Electrical resistance is due to scattering of electrons within a material. By analogy, consider how fast it takes you to drive from one town to another. Without obstacles on a freeway, you can proceed quickly. But if you encounter heavy traffic, accidents, road construction and other obstacles, you'll travel much slower.

Depending on its magnetic direction, a single-domain magnetic material will scatter electrons with "up" or "down" spin differently. When the magnetic layers in GMR structures are aligned anti-parallel, the resistance is high because "up" electrons that are not scattered in one layer can be scattered in the other. When the layers are aligned in parallel, all of the "up" electrons will not scatter much, regardless of which layer they pass through, yielding a lower resistance.

1.1.4. Application of GMR

The use of GMR-based data storage would play a major role in advancing the state of our technology. For example, in aviation and space applications, the non-volatile and radiation-resistant properties of GMR-based RAM (MRAM) could be exploited for

computer memories of aircrafts and satellites[1], thus promising better performance of satellites and aircraft navigation. The radiation resistant properties of MRAM also mean that it does not have to be shielded by lead-based packaging in high-radiation environments of space. Consequently, using GMR memories, aircraft and satellite designers can simplify their designs and reduce the overall weight.

GMR materials can achieve sensitivities to fields of perhaps as much as five times greater than conventional ferromagnetic metals. Consequently GMR materials are extremely useful for ultra-high-density data storage and as sensors for the detection of magnetic fields. Application of GMR materials is manifold. Some of the applications are:

GMR materials have tremendous potential for military and civil applications as Sensor:

- For example, GMR-based motion sensors, in tandem with a GPS[2], can be used for the electronic surveillance of international borders. GMR-based technology would also improve the missile guidance system.
- False positive detections account for a great part of the expense associated with unexploded ordnance (UXO) remediation. A GMR-based imaging detector would allow the operator to easily distinguish between UXO and benign objects (like shrapnel or spent bullets) that litter formerly used defense sites (FUDS).
- Poaching has been one of the biggest problems in wild life sanctuaries/national parks. The use of GMR-based motion sensors can be used for the electronic surveillance of these parks/sanctuaries.
- GMR-based sensors can be used for automotive antilock brakes, and auto-traction systems; motion and position sensors for electrical safety devices; current transformers or sensors for measuring direct and alternating current, power, and phase; automotive engine control systems; highway traffic monitors etc. The system operates by having magnets mounted on the wheel that pass by a GMR

[1] Power failure and ionizing radiation from space can destroy data in conventional semiconductor-based RAM

[2]Global Positioning System.

detector. The sensor measures the rate of wheel rotation and feeds the data to an on-board computer, which regulates the braking pressure to prevent a skid. GMR detectors like this are inexpensive, reliable, and very effective as position sensors.

Data Storage

- Very high density computer hard disks where five gigabits of binary information, about 90,000 pages of text, can be stored on one square inch.
- Non-volatile, radiation-resistant RAM (MRAM) in computers. MRAM devices would be smaller, faster, cheaper, use less power. It would also be much more robust in extreme conditions such as high temperature, or high-level radiation or interference than conventional semiconductor RAM.

Early in November 1997, IBM was the first company to announce GMR magnetic recording read heads in a family of disk drive products, designated Deskstar* 16GP [7]. First customer shipment began in January 1998. In these products, the use of GMR read heads allows the reading of extremely small magnetic bits at an areal density of 2.69 gigabits per square inch.

The largest impact of GMR materials will probably be for nonvolatile magnetic memory in computers, which is under development at several corporations within the United States, Japan, Germany, France, and the Netherlands. GMR materials are already the focus of intense research and development efforts at companies as wide-ranging as IBM, Kodak, Sony, Toyota, and Honeywell, among many others. Considering its manifold and strategic importance, it is imperative that R&D efforts in developing GMR materials be intensified.

1.2. Compositionally Modulated Materials (CMM) or Alloys.

Compositionally Modulated Alloys (CMA) materials are multilayered structures consisting of layer of pure metal or alloys. Such metal have wide potential applications owing to their unique technological properties, which differ considerably pure metals and

homogeneous alloys. These materials have promising magnetic [8-10], mechanical [11-13], ductility [12], wear [12, 14], electrical [15] properties.

CMA coatings and materials are two types micro- and macro-CMAs depending on the thickness of individual sub layers. Micro-CMAs are composed of thin sub-layers for which the changed properties presumably originate from atomic/electronic interaction between sub-layers. In macro-CMAs the sub-layers are so thick that atomic/electronic interaction become negligible. The improved propertied then originated from physical interaction between sub-layers, as in traditional composite materials. The division between micro- and macro-CMA materials depends on the particular properties being considered, but will often be in the interval 10-100 nm.

1.3. Manufacturing technique

CMA materials can be produced either by dry or wet processes.

1.3.1. Dry Processes

The dry processes, which are all based on vacuum technique, are chemical and physical vapour deposition, sputtering, molecular beam epitaxy, laser ablation and normal temperature evaporation technique.

1.3.2. Wet Processes

The wet processes are all electrochemical, using either the dual-bath or the single-bath deposition technique. Deposition of metallic, semi-metallic and ceramic CMA structures by dry process has been studied since 1940 [16]. The process has been found industrial application in the production of monochromators and reflectors. In the last decade, where industrial production of CMA structures has been considered seriously for a number of widely different applications, electrochemical deposition has received increasing attention. Production of CMA materials by electrodeposition has a number of advantages over the dry processes:

- It is a low cost process.

- Equipment is simple.
- Deposition rate is high (up to about 5μm per minute).
- Thick coatings can be deposited (>1000 μm)
- Deposition control is precise and with high reproducibility
- Completed geometries can be coated
- Since it is a cold process, the risk of interdiffusion between sub-layers is low

Solutions used in the wet processes often have complicated composition (metal salts, complexing agents, buffer, inert electrolyte, additives). Due to the high number of variables process optimization and control is complicated. Another disadvantage is that deposition can take place only on conducting materials. The elements in the bold letter in the periodic table in Fig. 1.1 represent metals that can be plated as pure metals from aqueous solutions.

Two techniques can be employed for the deposition of CMM and are discussed in the following sections.

1.3.2.1. The dual bath technique

Using the dual bath technique each sub-layer is plated in a separate solution. The sample is then cycled between two solutions. Thus it is possible to combine layers of two completely pure metals or alloys plating solutions, respectively. It is a simple technique in which readily available commercial solutions can be used.

The idea of producing CMA coating with the dual bath technique is not new. It is described as early as 1921 by Blum [17] who electrodeposited Cu-Ni, Cu-Ag and Cu-Cu CMA coatings. As a consequence of growing interest in producing CMA materials in the last decade, the dual bath technique has received renewed interest.

1a	2a	3b	4b	5b	6b	7b	8			1b	2b	3a	4a	5a	6a	7a	0
H 1																	He 2
Li 3	Bc 4											**B 5**	C 6	N 7	**O 8**	F 9	Ne 10
Na 11	Mg 12											Al 13	Si 14	**P 15**	**S 16**	Cl 17	Ar 18
K 19	Ca 20	Sc 21	**Ti 22**	**V 23**	Cr 24	**Mn 25**	**Fe 26**	**Co 27**	**Ni 28**	**Cu 29**	Zn 30	**Ga 31**	**Ge 32**	**As 33**	Se 34	Br 35	Kr 36
Rb 37	Sr 38	Y 39	Zr 40	**Nb 41**	**Mo 42**	Tc 43	**Ru 44**	**Rh 45**	**Pd 46**	**Ag 47**	**Cd 48**	**In 49**	Sn 50	**Sb 51**	**Te 52**	I 53	Xe 54
Cs 55	Ba 56	La 57	Hf 72	Ta 73	**W 74**	Re 75	**Os 76**	**Ir 77**	**Pt 78**	**Au 79**	**Hg 80**	**Tl 81**	**Pb 82**	**Bi 83**	Po 84	At 85	Rn 86
Fr 87	Ra 88	Ac 89	Rf 104	Ha 105	?? 106												
Lanthinide Series		Ce 58	Pr 59	Nd 60	Pm 61	Sm 62	Eu 63	Gd 64	Tb 65	Dy 66	Ho 67	Er 68	Tm 69	Yb 70	Lu 71		
Actinide Series		Th 90	Pa 91	U 92	Np 93	Pu 94	Am 95	Cm 96	Bk 97	Cf 98	Es 99	Fm 100	Md 101	No 102	Lr 103		

Figure 1.1. The periodic table of elements. The enhanced elements (in bold letter) can be electrodeposited as pure metals from the aqueous solutions. The elements in *italicized* letter can be plated as alloying elements.

A computer–controlled dual–bath plating machine has been developed [18]. The machine has equipped with two plating baths, two tanks of rinsing and spray activation and a bath for secondary drip rinsing. The sample is moved between the baths by a pneumatic transport system.

A more sophisticated construction of dual-bath system consists of a rotating dise exposed to solutions through two windows surrounded by gaskets [19]. In a variant of this construction the rotating dise is in contact with the solutions through two plating nozzles [20, 21]. Using these constructions it is possible to produce CMA coating with sub-layer thickness in the nanometer range, but only substrates with rotation symmetric geometry can be plated.

1.3.2.2.The single-bath technique

Using single bath technique, sub-layers are plated from one solution containing two or more elements forming the CMA deposit. The composition is modulated by changing the current /potential pulse and the hydrodynamic conditions. Usually the alloy solution contains a relatively precious metal (positive reduction potential) at lower concentration and a less precious (less positive or negative reduction potential) at a much higher concentration. The variant of pulse-deposition techniques are described below.

1.3.2.2.1. Dual-Current Pulse

The most common way of to produce CMA coating from the above-mentioned solutions, is to use the dual-current method, where the current is altered between a high and a low level. At low current density (low overpotential) only the precious metal is deposited. At high current density (high overpotential) the limiting current density (i_L) is exceeded for precious metals and less precious metal is deposited. Fig. 1.2 shows the dual-current pulse waveform for CMA electrodeposition. This method was first described by Cohen et al., [15].

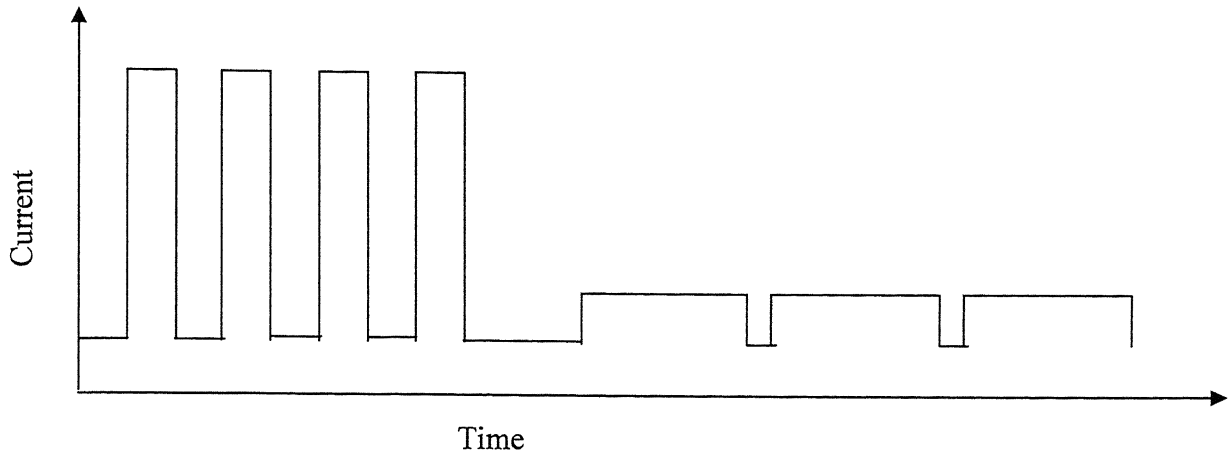

Figure 1.2. Dual-Current pulse waveforms for electrodeposition of CMA coatings.

1.3.2.2.2. Dual-Current Pulse with Current Interruption

The dual-current method has been modified by introducing a period of current interruption following the high current pulse as shown in Fig. 1.3 [22]. The current interruption improves the sharpness of the transition zone between the sub-layers.

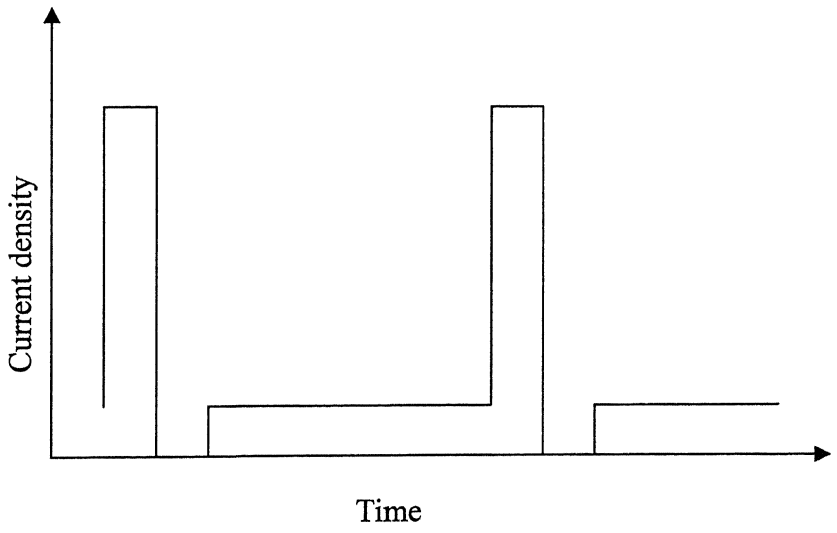

Figure 1.3. Dual-Current pulse with current irruption waveforms for electrodeposition of CMA coatings.

CHAPTER II

LITERATURE REVIEW

A summary of the research activities in the development of GMR materials, both by vacuum deposition and electrodeposition is presented in this chapter

2.1. Previous Works on Vacuum Deposition

An experimental survey of GMR for Co/Ru, Co/Cr, and Fe/Cr sputtered superlattice structures revealed that the saturation magnetoresistance oscillates with spacer layer thickness [23] Here the GMR effect mirrors the oscillation of the nature of magnetic coupling Only those multilayers for which the initial interlayer coupling is antiferromagnetic display significant giant GMR effects. It disappears for samples with an initial ferromagnetic coupling. The oscillation period was found to be just a few atomic layers, typically about 10 A, but varying up to ~20 A

The application of a strong enough magnetic field usually parallel to the plane of the layers changes the arrangement of the magnetization. The antiferromagnetic coupling is overcome, and the magnetic moments of all the ferromagnetic layers are forced to lie in the same direction Simultaneously, the electrical resistance of the sample, both in the plane of the layers and perpendicular to it, decreases. This decrease can be a few percent, as in Co/Ru, or can exceed 110% [7] at room temperature as in Co/Cu multilayers. This decrease occurs for almost all configurations regardless of the direction of the current, the directions of the electric and magnetic fields, the chemical composition of the spacer and the structure of the interface as long as the magnetic arrangement changes from antiparallel to parallel upon application of the magnetic field.

Parkin and coworkers [24] showed that polycrystalline magnetic multilayers, prepared by the widespread technique of sputtering, had properties similar to those of single-crystalline multilayers prepared by MBE. It thus raised questions of the influence

of crystalline orientation, interface roughness, and structural quality of the multilayers on interlayer coupling and GMR.

While GMR was originally observed for layered elemental metals, it was found to occur for ferromagnetic permalloy ($Ni_{80}Fe_{20}$) [25]. In the case of permalloy (Py), the magnetoresistance ratio is reduced by compositional intermixing at Py/Cu interfaces [26] This is attributed to reduction of magnetization in the mixed layers

2.2. Previous Works on Electrodeposition

Leisner and coworkers [27] have reviewed electroplating techniques used for depositing multilayered structures (MLS), also known as compositionally modulated alloys (CMA). The single-bath technique is considered the most promising technique for producing MLS. In the single-bath technique, sub-layers are plated from one solution containing two or more elements forming the MLS. The composition is modulated by changing the current/potential pulse or the hydrodynamic conditions. The most common way to produce MLS is to use the dual current method, where the current is alternated between the high current and low current level. At low current densities only the precious metal is deposited while the less precious metal is deposited at high current densities. The dual current method has been modified by introducing a period of current interruption/reversal following the high current pulse. The current interruption/reversal improves the sharpness of the transition zone between the sub-layers Unfortunately, the papers reviewed by Leisner and coworkers [27] did not shed much light on the GMR characteristics of the electrodeposited MLS. Consequently, the status of MLS with specific reference to GMR materials is reported in the ensuing paragraphs.

Lenczowski and coworkers [28] investigated the structural and electrical characterization of electrodeposited Co/Cu multilayers grown from a single bath containing $CoSO_4$ and $CuSO_4$. A high degree of crystallographic orientation and superlattice coherence was found in the growth on (100) and (111) – oriented substrates.

A maximum GMR of 14% was measured. It was also observed that the magnetoresistance (MR) at room temperature is dominated by the GMR effect for copper layer thicknesses (d_{Cu}) greater than 3 nm and by AMR effect for $d_{Cu} < 2.5$ nm Experiments also showed that GMR gradually diminished with decreasing d_{Cu} less than 4 nm In addition the use of a leveling agent had a catastrophic effect on the structural quality of the multilayers and on the magnitude of MR.

Jyoko and coworkers [29] electrodeposited Co/Cu multilayers on a Pt (111) substrate under potential control Such a multilayered structure containing a nominal Cu spacer layer thickness of 3.2 nm exhibits a large saturation MR of more than 18% at room temperature.

Bonhote and Landolt [30] produced multilayered Ni-Cu deposits on rotating cylinder electrodes from a citrate electrolyte The modulation was 20 nm and 10 nm for Ni and Cu sublayers, respectively Multilayered deposits of the same modulation were prepared using two different current densities for deposition of the copper sublayer, corresponding to kinetic or mixed (mass transport and kinetic) control of the electrode reaction. The microstructure of the Ni-Cu multilayer deposit was determined using X-ray diffraction, scanning electron microscopy and transmission electron microscopy. Depending on the applied current density, and hence overpotential, for copper deposition a columnar structure of large grains, oriented in the [110] direction, or an equiaxed structure comprised of small non-oriented grains were observed. The results show that by modifying the deposition conditions for copper it is possible to alter the grain size of the multilayered alloy without changing the modulation

Schwarzacher and coworkers [31] showed that GMR is sensitive to whether deposition is carried out under potentiostatic or galvanostatic control, and the choice of substrate. They observed that texture of Co-Ni-Cu/Cu superlattices grown on polycrystalline (100)-textured Cu plates and (110)-textured Cu foil under potentiostatic control depended on that of the substrate, while comparable superlattices grown under

galvanostatic control had a predominantly (111) texture. The films grown under galvanostatic control generally exhibited AMR or smaller GMR.

Cziraki and coworkers [32] correlated microstructure and giant magnetoresistance in electrodeposited Ni-Cu/Cu multilayers. Giant magnetoresistance (GMR) was observed in pulse-plated $Ni_{81}Cu_{19}$/Cu multilayers with a maximum GMR value of about 2% for Ni-Cu layer thicknesses around 2 to 3 nm A columnar growth of the multilayers was detected by transmission electron microscopy. The column width (grain size) was the largest for multilayers with the maximum GMR

Jyoko and coworkers [33] grew multilayered Co/Pt nanostructures on a Cu (111) single-crystal substrate by electrodeposition under potential control. This nanostructure exhibited a remnant perpendicular magnetization and a large coercivity, which was a function of the deposition overpotential. GMR and oscillatory antiferromagnetic coupling were also observed in a FCC (111) textured Co/Cu multilayered nanostructure. Moreover, a large saturation MR of more than 20% was achieved at room temperature for a heterogeneous Co-Cu alloy, which consisted of ultrafine Co-rich, clusters in a Cu matrix

Toth-Kadar and coworkers [34] used galvanostatic electrodeposition to produce $Ni_{81}Cu_{19}$/Cu multilayers from a sulphate/citrate electrolyte. TEM studies showed that Ni-Cu/Cu multilayers grew in a columnar form and that the columns exhibited a large number of stacking faults and twinnings Both GMR and AMR contributions were observed for most $Ni_{18}Cu_{19}$/Cu multilayers. For increasing magnetic layer thicknesses, the AMR contribution became more and more dominant and the MR curves approached those obtained for the bulk $Ni_{18}Cu_{19}$ alloy.

Alper and coworkers [35] grew a series of Co-Ni-Cu/Cu multilayers from a sulphamate electrolyte which exhibited GMR of up to ~20%, the largest GMR being obtained for the thinnest Cu layers (~7 Å). According to Alper and coworkers this result showed that magnetic multilayers prepared by electrodeposition are competitive with

those prepared by the costlier vacuum processes. Alper and coworkers [38] and Lenczowski and coworkers [28] have attributed the suppression of GMR in Co-Ni-Cu/Cu (at high pH values) and Co/Cu systems respectively to defects ("pin holes") in the Cu, or too much interfacial roughness. Interfacial roughness was attributed to the deposition of copper by the exchange reaction $Co + Cu^{2+} = Co^{2+} + Cu$.

Peter and coworkers [36] electrodeposited Co-Cu/Cu multilayers under galvanostatic control from a $CoSO_4 - CuSO_4$ electrolyte Atomic force microscopy, X-ray diffraction and Transmission electron microscopy were used to study the sample structure and morphology They established that a significant part of the Cu layer was produced by the exchange reaction even under current interruption/reversal conditions. Significantly, Peter and coworkers' experiments also showed that the GMR of the multiplayer deposit also decreased with increasing bilayer number (sample thickness). This loss of GMR was attributed to the structural disorder developed during electrodeposition More specifically, the substrate side showed a strong crystallographic orientation, which becomes less pronounced towards the solution side.

In order to make it easier to integrate electrodeposited magnetic nanostructures and conventional semiconductor-based electronics, a number of groups have studied the electrodeposition of magnetic multilayers on Si and GaAs. Co-Ni-Cu/Cu multilayers were potentiostatically electrodeposited by Kasyutich and coworkers [37] on to n-doped GaAs substrates with two different crystal orientations, (001) and (111). X-ray diffraction and transmission electron microscopy showed that epitaxial growth occurred on GaAs (001), with either the {001} or {211} planes parallel to the substrate. Epitaxial growth did not occur on GaAs (111). Here the multilayers grew preferentially with the {111} planes parallel to the substrate, but the crystallites had no preferred orientation in plane. Multilayers grown on the two crystal orientations exhibited GMR For small Cu layer thicknesses, $t_{Cu} < 20$ A, the GMR was suppressed for both crystal orientations. For $20 \text{ A} < t_{Cu} < 30$ A, GMR was much greater for multilayers electrodeposited on GaAs (001) than for those on GaAs (111), while for larger layer thicknesses, the GMR for both substrate orientations was similar. Kasyutich and coworkers [37] have explained the

difference in GMR behavior qualitatively by the presence of different numbers of defects producing different degrees of ferromagnetic coupling in the two sets of multilayers

Hadian and Gabe [39] electrodeposited Ni from a Watts bath using both pulse and continuous current They observed that nickel deposits were adherent with bright texture and fine grains at high current density but dull, thin, and coarse-grained at lower current density. Hadian and Gabe [39] further observed that the use of pulse current improved adhesion The magnitude of overpotential in the activation polarization range is the driving force for nucleation Higher the applied potential (or overpotential), greater would be nucleation sites resulting in smaller grains.

Ghosh et al [40], electrodeposited nanocrystalline Ni-Cu alloy by pulse plating They observed bright, smooth and coherent deposits in the frequency range of 10-100 Hz. However, with a further increase in pulse frequency, dull, grey and rough deposits were obtained. Ghosh and coworkers [40] also observed that with increasing duty cycle, the quality of deposit changes from very smooth, bright to non-metallic black and powdery.

2.3. Objectives of the Present Work

The objective of this research has been to:

1 Identify optimum conditions such as pulse parameters and electrolyte composition for the electrodeposition of Cu-Ni multilayer from a single bath.

2. Extensive structural characterization of multilayers.

CHAPTER III

EXPERIMENTAL APPARATUS & PROCEDURE

Introduction

Pulse electrodeposition of Cu-Ni multilayer (CNM) was carried out with the single bath technique. This section deals with the experimental setup and parameters used in the experiment.

3.1. Experimental Set up

The experimental setup for electroplating consisted of Potentiostat, Computer, Electroplating Reactor, Ammeter, and Voltmeter as shown in Fig. 3.1.

3.1.1. Potentiostat

The potentiostat was used for producing rectangular current and voltage pulses for electrodeposition of Ni and Cu multilayer. The Potentiostat (Potentiostat/Galvanostat Model 263A, *EG&G INSTRUMENTS, Princeton Applied Research*) was interfaced with host a computer (Pentium III micro-processor), where the user can program suitable rectangular or square pulses. With this Potentiostat, pulse parameters such as applied voltage (0V to ±4V), peak current (up to 1 Ampere), pulse frequency (0.0001Hz to 2000Hz) and duty cycle (0% to 100%) can be varied.

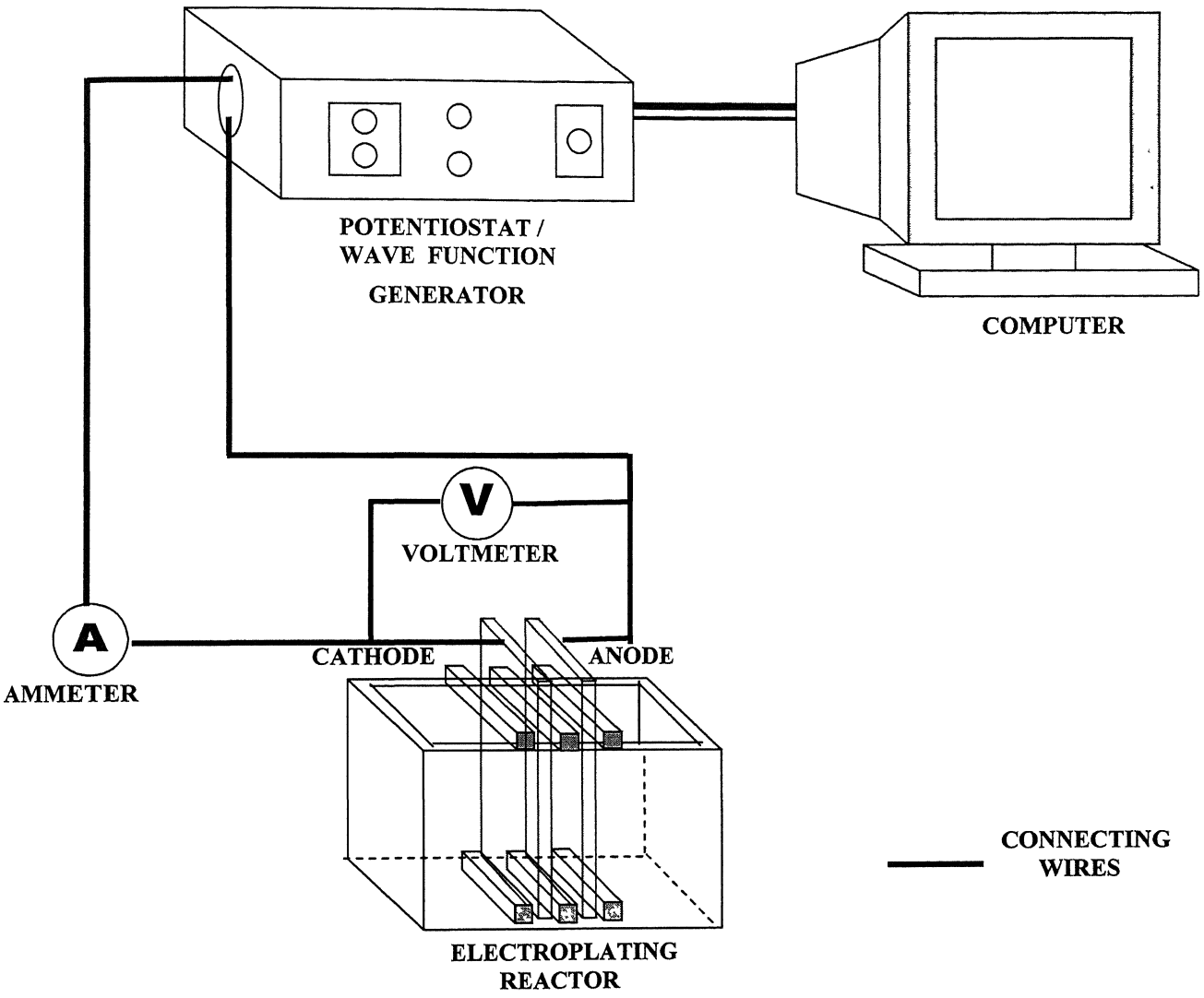

Figure 3.1. The schematic diagram of a computer controlled set up for deposition of CMM of copper and nickel.

3.1.2. Electroplating Reactor

This electroplating reactor was made of Perspex, the exact dimensions of which are shown in Fig. 3.2. Specially-designed grippers are used to hold the electrodes firmly in places. The design of the grippers was such that the inter-electrode distance (IED) can be varied according to the requirement.

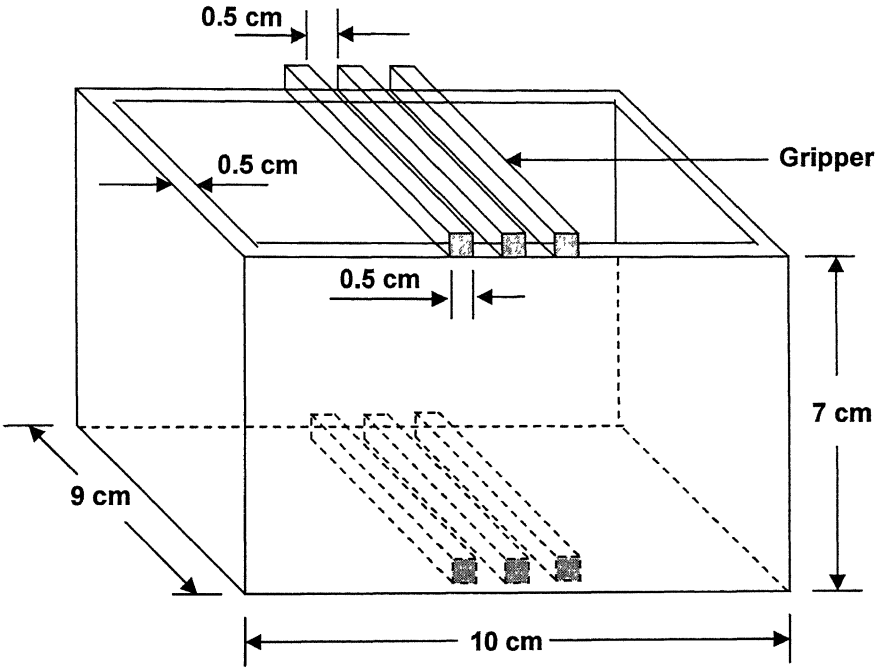

Figure 3.2. The schematic diagram of the electroplating reactor.

3.1.3. Electrode

A stainless steel and copper sheets were used anode and cathode respectively. The dimensions of the cathode and anode are 12 cm x 7.5 cm x 2 mm. In all experiments, the deposited area was 22.5 cm^2.

The reactions that occur during plating are as follows:

Reactions:

The reactions at the time of Cu depositions are-

At Anode:

$$2H_2O \leftrightarrows O_2 + 4H^+ + 4e$$

At cathode:

$$Cu^{++} + 2e \leftrightarrows Cu$$

The reactions at the time of Ni deposition are-

At anode:

$$2H_2O \leftrightarrows O_2 + 4H^+ + 4e$$

At Cathode:

$$Ni^{++} + 2e \leftrightarrows Ni$$

$$H^+ + e \leftrightarrows \frac{1}{2}H_2$$

3.1.4. Electrolyte

Electroplating of Cu and Ni was carried out using the following electrolyte [38]:

$NiSO_4$, $6H_2O$ -------- 280 g/l
$CuSO_4$, $5H_2O$ -------- 2 g/l
H_3BO_3 ---------- 30 g/l
$MgSO_4$, $7H_2O$ ------- 120 g/l

One or two drop of concentrated H_2SO_4 was added to maintain the pH of the electrolyte below 3. The role of the additives such as H_3BO_3 and $MgSO_4$, $7H_2O$ are stated below.

$MgSO_4$, $7H_2O$: Magnesium Sulphate was used to increase the conductivity of the bath.

H_3BO_3: Boric acid serves as a weak buffer in the plating solution. Its principle effect is that of controlling the pH of the electrolyte. In the absence of buffer, nickel deposit at ordinary temperature tends to be hard, cracked and pitted. Furthermore, Boric acid helps in producing a planer deposit.

3.2. Pulse Parameters

Pulse parameters used in the experiments are schematically shown in Fig. 3.3.

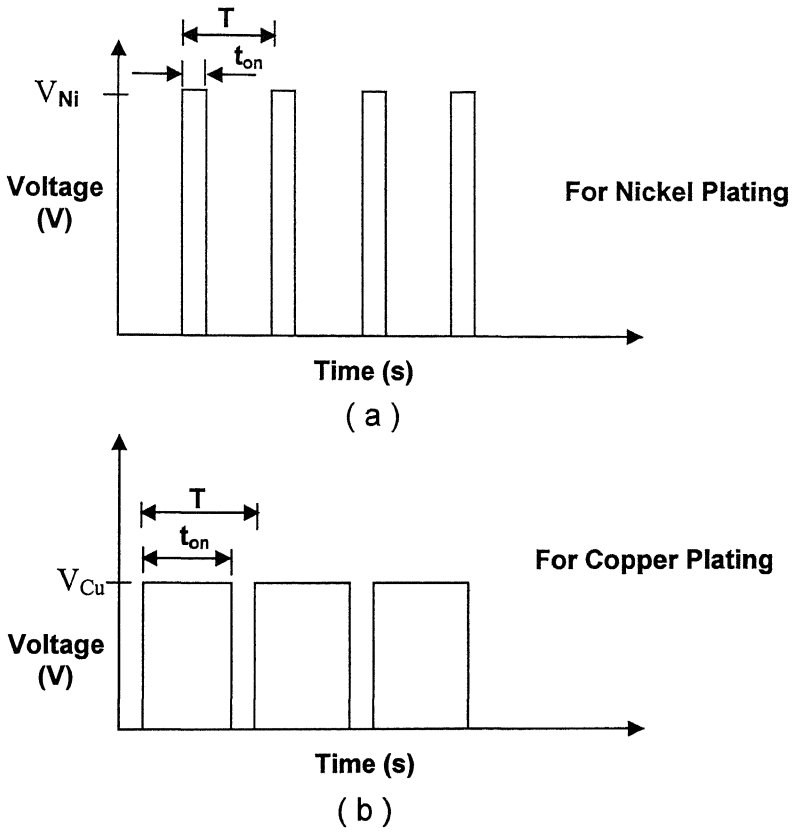

Figure 3.3. Potential pulse waveforms for electrodeposition of CMM coating: (a) potential pulse for nickel plating (b) potential pulse for cooper plating.

3.2.1 Voltage

Nickel and Copper can be alternately deposited from a single electrolyte. The standard deposition potential, of Ni and Cu are -0.25V and 0.34V respectively. The minimum deposition potential for Cu and Ni (V_{Cu} and V_{Ni}) was calculated as followed:

$$V_{Cu} \text{ (or } V_{Ni}) = |E_{Cell}| + I.R_{Solution}$$

$$= |E_{Cell}| + I.(\rho . L/A) \quad \text{----------(1)}$$

Where,

E_{Cell}= Standard Cell potential for nickel and copper deposition.

I = the current passing through the cell.

ρ = Resistivity of the Electrolyte= 1/Conductivity

L = Distance between the electrodes.

A = Area of deposition.

Activation overpotential is not significant for metal deposition reactions. The need for smooth and planer deposit implies that deposition should not be mass transfer controlled and hence concentration overpotential was ignored. Details of the calculations are given in Appendix-I.

The applied voltage (see in Fig. 3.3) was varied as follows:

V_{Cu} = 1V - 1.498V

V_{Ni} = 2V - 3.25V

3.2.2. Duty Cycle

Duty cycle (DC) is defined as:

$$\text{Duty Cycle (\%)} = \frac{t_{on}}{T} \times 100$$

A number of experiments were conducted to determine the range of duty cycle for both copper and nickel plating. The operating duty cycle was varied as follows:

For Cu: 70% - 90%

For Ni: 33.33% - 50%

3.2.3. Pulse Frequency

Pulse frequency is expressed as:

Pulse frequency (f) = 1/(On Time + Off Time)

= 1/T

Frequency range at which Cu and Ni deposition took place was:

For Cu: 0.025 Hz – 2 Hz

For Ni: 0.069 Hz – 4.17 Hz

3.3. Sample Preparation

Composition Modulated Multilayers of Cu-Ni were electroplated on a flat copper substrate, which was used as cathode. A stainless steel sheet was used as anode. The flat sheets of copper were first degreased in an alkaline solution and then cleaned in distilled water. Then mechanical polishing was done by belt grinder and final paper polishing was done on different emery papers 1/0, 2/0, 3/0 to a mirror like finish. After mirror like finish, the substrates were washed with methanol. Before the experiments, both anode and cathode were taped with a sallow tape on the back face for minimizing the loss of current at the time of electrodeposition.

The cathode, where the depositions of Ni and Cu platings were done was taken for characterization, which is discussed in the following section.

3.4. Measurement of Current Efficiency (C.E.)

The cathodic current efficiency for Cu and Ni was calculated by the equation given below.

C.E. = (Weight of metal deposited)/ (Weight to be expected from Faraday's law) x 100

$$C.E. = \frac{(W_2 - W_1)}{I.e.t/96496} \times 100$$

Where,

W_1 = Weight of cathode before deposition, in gm

W_2 = Weight of cathode after deposition, in gm

I = Current passing through the cell, in Amperes

e = Chemical equivalent weight of Cu and Ni

t = deposition time, in second

3.5. Macroscopic Deposit Characterization

The nature of deposition whether it was dull or dark or bright or shining were examined visually or by scanning electron microscope. The adherence of the deposit on the substrate was determined by rubbing the deposit with emery paper. If the plating peeled off easily from the substrate then it is non-adherent, otherwise it is defined as adherent. Powdery characteristics of deposit was determined by rubbing it with a finger. If the deposit came off easily, then it was defined as powdery.

3.6. Multilayer Characterization

The structural characterization of Cu-Ni multilayer such as thickness of individual Cu and Ni sub-layers, total thickness of deposition, number of sub-layers and deposition morphology were done by Scanning Electron Microscopy. **But due to unavailability of SEM, the microstructure of deposition could not be ascertained.** X-Ray diffraction was carried out for detection of Cu and Ni and their grain size. Magnetic Measurement

also done by parallel field vibrating sample magnetometer (VSM) for diffusion studies between the sub-layers.

3.6.1. Scanning Electron Microscopy (SEM)

3.6.1.1. Sample Preparation for SEM

The necessary few steps for the preparation of SEM sample from a Electrodeposited Cu-Ni multiplayer on copper substrate are shown below-

- Sample Cutting
- Cleaning and Drying
- Embedded in Epoxy (Cold Mounting)
- Polishing and Etching of cross sections
- Carbon coat using Ion Beam Deposition
- Examine using SEM

3.6.1.1.1. Sample Cutting

- Sample was cut by an area of 1cm x 1cm.
- Cutting Mill was used for cutting.
- Hack Saw was avoided for consuming time.
- Cutting must be done carefully to avoid peeling off coating.

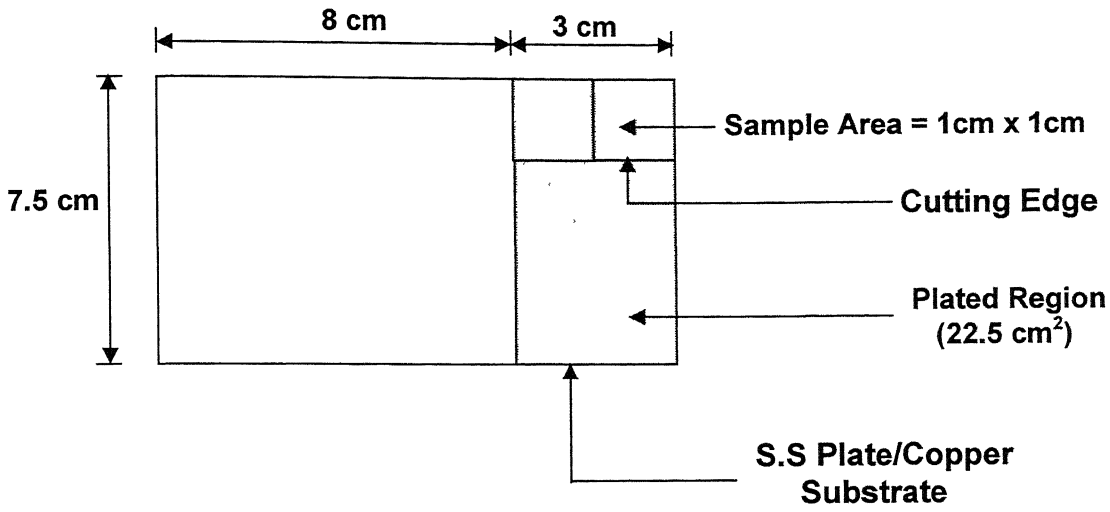

3.6.1.1.2. Cleaning and Drying

- The samples must be free of oil and loose particles. These were removed by alkaline solution.
- Air-drying was done to remove water from the sample.

3.6.1.1.3. Embedded in Epoxy (Cold Mounting)

- Samples were mounted, which allows them to be placed in the instrument.
- The most common mounting, 1 inch round mounting was done. For observing the thickness of the thin deposition the transverse section (the cutting edge) was placed downwardly. Then the epoxy was filled in the moulds with some acids. Thirty minutes were allowed for full solidification.

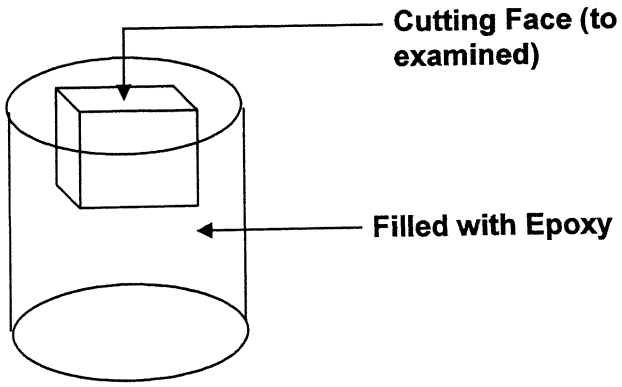

3.6.1.1.4. Polishing and Etching of cross sections

- Saw marks were removed by grinding with 400 grit followed by 600 grit sandpaper.

- Then the polishing was done on different emery papers 1/0, 2/0, 3/0, and 4/0 respectively.

- Final polishing was done on a lap wheel with (6, 3, 1, and 0.25) μm diamond paste or fine alumina (10 μm) for 2 to 5 minutes each. After each polishing, the specimen is cleaned using a clean cloth and after the final polishing step, ethanol is used to remove any residual polishing compound.

- Etching was done by the solution containing 1 g $K_2Cr_2O_7$, 2 ml H_2SO_4 and 0.1 ml HCl. This solution etched Copper selectively, allowing the visualization of the layered structure of the Cu-Ni multilayer.

3.6.1.1.5. Carbon coat using Ion Beam Deposition

- The final polished specimen was coated with carbon to provide a conductive surface for viewing in the SEM. Because this conductive coating prevents charging under electron bombardment.

- A table of carbon coating thickness (in Angstroms) against interference color:

  150 – Orange
  200 – Indigo red
  250 – Blue
  300 – Bluish green
  350 – Greenish blue
  400 – Pale green
  450 – Silver gold

- The carbon coating was done for 1 hr.

3.6.1.2. SEM Analysis

The structural characterization like the thickness of individual Cu and Ni sub-layers, total thickness of deposition, number of sub-layers and deposition morphology were studied by using JSM-840A Scanning Electron Microscope. The samples were placed vertically by fixing them on to an Aluminum block using an adhesive. This aluminum block was placed on the specimen holder and suitable packing was used to prevent any movement of sample. An aluminum foil was placed between the sample and aluminum block, which touches the conducting coating of sample. The structure was examined at magnification 1000X to 10000X.

But due to unavailability of SEM, the extensive microstructural characterization of deposits could not be done.

3.6.2. X-Ray Diffraction Analysis

3.6.2.1. Sample Preparation for XRD

- The dimensions of samples used for XRD analysis was 1 cm x 1 cm x 2mm.
- The top face (where the Cu-Ni coating is deposited) was examined for XRD analysis.
- The top face was thoroughly washed with distilled water before XRD analysis.

3.6.2.2. Analysis

The X-Ray analysis was done by X-Ray powder diffractometer ISO-DEBYEFLEX 2002. The flat sample was placed horizontally on the sample holder for analysis. The copper target was used, which has a K_α wavelength of 1.54056 Å. The scan rate of the analysis was 3.0°/min. The analysis was done between the angles 35° to 100°.

The intensity of different peaks and the data were compared with standard JCPDS files for various elements and compounds.

The grain size of the films was estimated by using the Scherrer formula-

$$t = \frac{0.9\lambda}{BCos\theta_B} \qquad \text{.....(1)}$$

Where,

t = grain diameter, in meter

λ = Wavelength of monochromatic X-ray beam, in meter

B = full width at the half maximum of the peak, in radian

θ_B = Bragg angle, in degree

The grain size of nickel and copper electrodeposits were calculated from the X-ray diffraction patterns. The details of the calculations are given in the Appendix-IV.

3.6.3. Magnetic Measurement

Systematic measurement of the magnetization, by means of a parallel field Vibrating Sample Magnetometer (VSM), allow a complete characterization of the diffusion process within the CMMs.

3.6.3.1. Sample Preparation

- Sample was cut into dimension of 2mm x 2mm x 2mm.
- Degreasing and cleaning were done.
- Mechanical polishing (roll grinder polishing) was done for proper fitting of the sample in the sample holder of VSM.

3.6.3.2. Experimentation

The magnetic measurements were performed on two 1080nm and 3269 nm thick Cu-Ni CMM having different Cu and Ni sub-layers thickness and sublayer [Sample 1, (Ni 300 nm/Cu 60 nm) x 3 times and Sample 2, (Ni 407 nm/Cu 60 nm) x 7 times]. The magnetization was measured for an applied field of 1260 Oe; by means of parallel field Vibrating Sample Magnetometer (VSM). Fast cooling interrupted the diffusion. The

magnetization was measured from about 435°C (for sample 1) and 400°C (for Sample 2) to reference temperature 25°C.

CHAPTER IV

RESULTS AND DISCUSSION

Introduction

The Effect of pulse parameters such as applied voltage, frequency, duty cycle, number of cycles, and electrolyte composition and pH on the quality of Cu and Ni electrodeposit will be discussed in this chapter

4.1. Effects of Pulse Parameters

4.1.1. Effect of Applied Voltage

Table 4 1 and 4 2 show the effect of applied voltage on the deposition of Ni and Cu respectively. The operating pulse frequency and duty cycle listed in tables 4.1 and 4.2 were determined from preliminary experiments

Table 4 1 shows that Ni deposits above 2.7 V at a frequency of 0.167 Hz and 33 33% duty cycle. Initially the deposit is dark and non-adherent. However, with increasing voltage adherent and bright deposit are obtained. As stated before, because of the unavailability of SEM, the microstructure of the deposit could not be ascertained However, the effect of voltage on the nature of deposit can be explained based on the study by Hadian and Gabe [39] Hadian and Gabe [39] electrodeposited Ni from a Watts bath using both pulse and continuous current. They observed that nickel deposits were adherent with bright texture and fine grains at high current density but dull, thin, and coarse-grained at lower current density. Hadian and Gabe [39] further observed that the use of pulse current improved adhesion. The magnitude of overpotential in the activation polarization range is the driving force for nucleation. Higher the applied potential (or overpotential), greater would be nucleation sites resulting in smaller grains. Thus, in the voltage range 2.91V to 3.3V, it is expected that our deposit had a fine-grained microstructure, the results that seems to be confirmed by X-ray diffraction (see Table 4 3)

In case of Copper electroplating, the deposition is bright and adherent between the potential range 1 002V to 1.498V, the mechanism is similar to that of nickel. After that the deposition was semi-bright and becomes non-adherent, dark and dull. But as the potential is increased above 1.812V, the deposition becomes powdery, dark and dull appearances as shown in Table 4.2. This is because as the applied potential increases, the cathodic current density (i_C) increase and it approaches to pulse limiting current density (i_{PL}) In this voltage range (1.812V to 2 123V), the deposition of Cu is mass transfer controlled, which first causes non-adherent, dull and later powdery.

For nickel electroplating, the best operating voltage varies between 2.91V to 3.287V for bright, shining and adherent deposition The best operating peak voltage for copper deposition varies between 1.062V to 1.498V Fig. 4.1 and 4.2 show typical micrograph of (i) bright and shining and (ii) powdery deposit.

Table 4 1 Effect of applied voltage on the electro-deposition of Nickel at pulse frequency, duty cycle and number of cycles of 0 167 Hz, 33.33% and 15 respectively.

V_{Ni} (V)	Peak Current (A)	Surface Appearance
2 197	0.08	No Ni-deposition.
2 28	0 12	No Ni-deposition.
2 39	0.16	No Ni-deposition.
2.534	0.18	No Ni-deposition
2 61	0 22	No Ni-deposition
2 69	0.26	No Ni-deposition
2 74	0 38	Non-adherent, dull and dark
2 84	0.42	Adherent, semi-bright
2.91	0 46	Adherent, bright, shining
2 967	0.56	Adherent, bright, shining
3.07	0.62	Adherent, bright, shining
3.12	0.68	Adherent, bright, shining
3.173	0 78	Adherent, bright, shining
3.225	0.88	Adherent, bright, shining
3 287	0.94	Adherent, bright, shining

Table 4 2 Effect of applied voltage on the electro-deposition of copper at pulse frequency, duty cycle and number of cycles of 0 10 Hz, 90 % and 15 respectively.

V_{Cu} (V)	Peak Current (A)	Surface Appearance
0 753	0 002	No Cu deposition
0.875	0 004	No Cu deposition
1.002	0.005	Adherent, bright
1.062	0 007	Adherent, bright
1 126	0 008	Adherent, bright
1 251	0 010	Adherent, bright
1 373	0.014	Adherent, bright
1.498	0.017	Adherent, bright
1 589	0 019	Adherent, semi-bright
1.742	0 025	Adherent, Semi-bright
1 812	0.027	Non-adherent, dark, dull
1 912	0.031	Powdery, dull and dark
2.123	0.043	Powdery, dull and dark

Table 4.3. Effect of applied potential on grain size of Cu and Ni.

Applied Potential (Volt)	Grain Size (Å)
For Ni 2.84	68
For Cu: 1 114	69
For Ni. 2 91	56
For Cu: 1 245	62
For Ni. 2.97	51
For Cu: 1 298	56
For Ni. 3 12	41
For Cu: 1.369	39

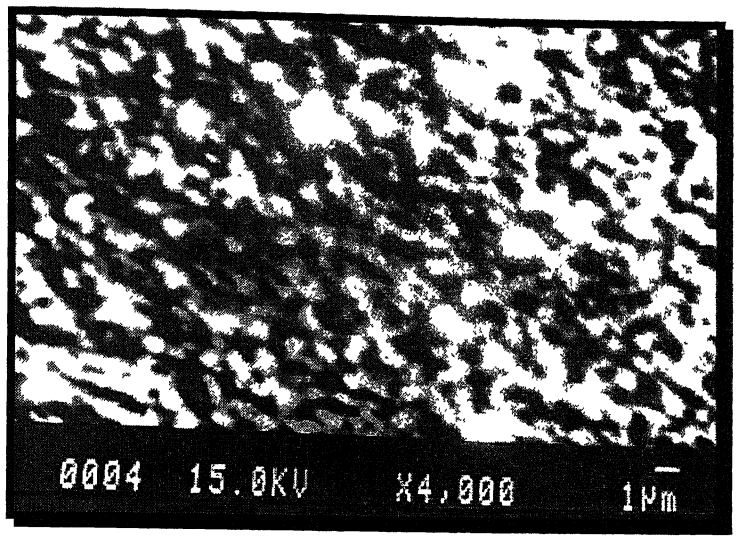

Figure 4.1. The EPMA micrograph at X 4,000 shows typical bright and shinning surface appearance of nickel deposition on the copper substrate.

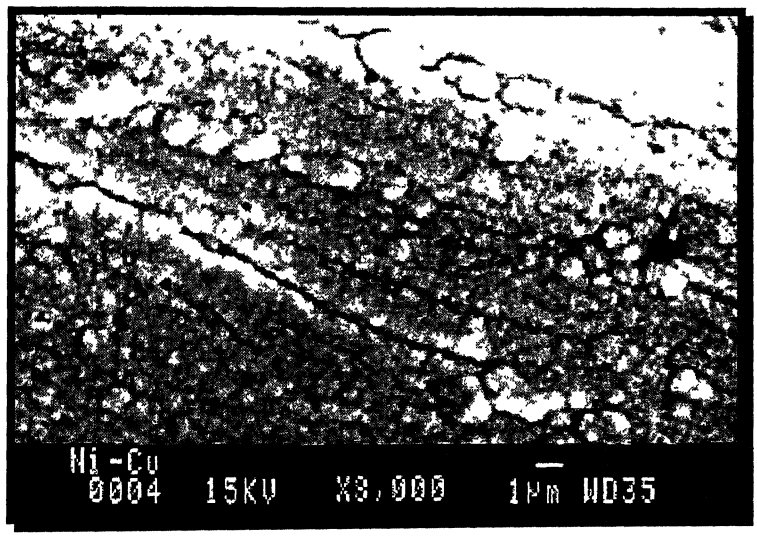

Figure 4.2. The SEM micrograph at X 3,000 shows a typical powdery deposition of copper on the copper substrate.

4.1.2. Effect of Pulse Frequency

Tables 4 4 and 4 5 show the effect of pulse frequency on the deposition of Ni and Cu respectively.

Frequency is one of the most important parameter for electrodeposition of Cu and Ni Both Cu and Ni plating depends on pulse frequency. The deposition of Cu and Ni occurs on the cathode surface at pulse on-time The mechanism of deposition consists of two processes First the charging of double layer to the deposition voltage (as shown in Fig 4 3) and then the deposition of metal occurs. At a fixed duty cycle, very high frequency results in lower pulse on-time (t_{on}). At low pulse on-time, the double layer is not fully charged to the deposition potential. This causes no deposition of Cu and Ni at high frequencies (16.7 Hz)[1] Dull, dark and semi-bright deposit of Ni occurs between 4 17 Hz and 0 833 Hz Under these conditions the Electric Double layer (EDL) at the cathode is partially charged, resulting in lower overpotential and consequently larger grain size At frequency below 0.278 Hz, bright and shining deposit is referred probably because the double layer can be charged to a higher voltage and hence higher overpotential leading to finer grains, as discussed in the previous section.

Good copper deposits were obtained below a frequency of 1.25 Hz. Cu deposition started at 2 Hz as shown in Table 4.5 In the frequency range from 2Hz-1.667Hz, the Cu depositions were adherent but semi-bright. Similar results were obtained by Ghosh et. al [40], who electrodeposited nanocrystalline Ni-Cu alloy by pulse plating. Ghosh and co-workers [40] observed bright, smooth and coherent deposits in the frequency range of 10-100 Hz However, with a further increase in pulse frequency, dull, grey and rough deposits were obtained. At very low frequencies (0 10 Hz for Cu deposition and 0.167Hz for Ni deposition) larger on time allows double layer to get fully charged to deposition voltage and thus both Ni and Cu platings were bright, shining and adherent.

[1] The total number of cycles in Tables 4.4 and 4.5 were varied to ensure that the total charges passed during deposition of Ni and Cu remain constant.

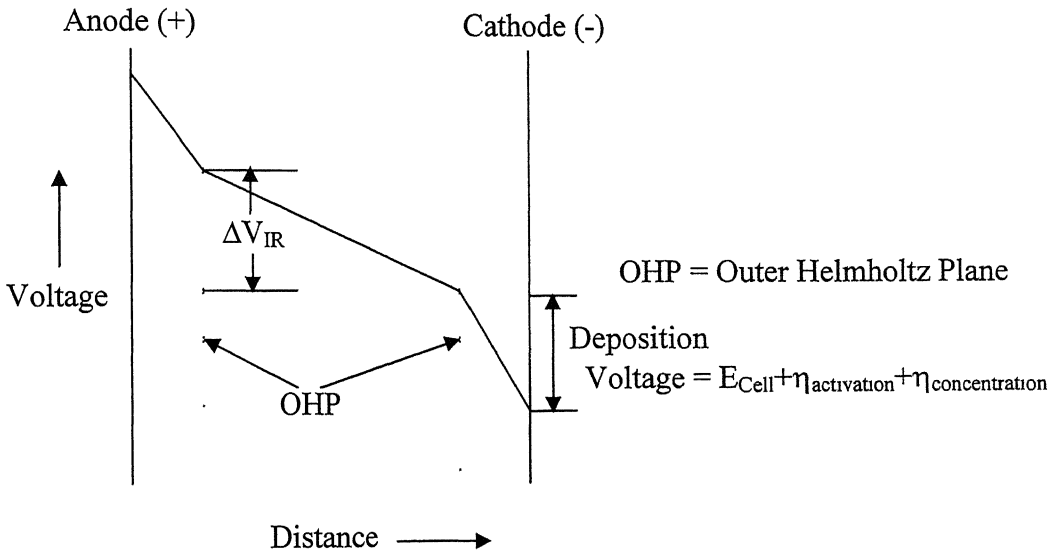

Figure 4.3. Variation of potentials across the electrode.

Table 4.4. Effect of pulse frequency on the electro-deposition of Nickel at V_{Ni} = 2 95 V and duty cycle of 33.33%

Frequency (Hz)	Surface Appearance	No. of Cycles
16 7	No Ni-deposition.	1500
8 33	No Ni-deposition.	750
4 17	Non-adherent, dull, dark	375
3 7	Adherent, dull, dark	334
3.33	Adherent, dull, dark	300
2 09	Adherent, dull, dark	190
1.67	Adherent, semi-bright	150
0.833	Adherent, semi-bright	75
0 278	Adherent, bright, shining	25
0 167	Adherent, bright, shining	15
0.139	Adherent, bright, shining	13
0 069	Adherent, bright, shining	7

Table 4.5. Effect of pulse frequency on the electro-deposition of Copper at V_{Cu} = 1.245 V and duty cycle of 90%.

Frequency (Hz)	Surface Appearance	No. of Cycles
16.7	No Cu deposition	2500
10.00	No Cu deposition	1500
5.00	No Cu deposition	750
2.50	No Cu deposition	375
2.00	Adherent, semi-bright	300
1.667	Adherent, semi-bright	250
1.25	Adherent, bright	190
0.625	Adherent, bright	95
0.313	Adherent, bright	48
0.157	Adherent, bright	24
0.100	Adherent, bright	15
0.050	Adherent, bright	7
0.025	Adherent, bright	3

4.1.3. Effect of Duty Cycle

Tables 4 6 and 4.7 depict the effect of duty cycle (DC) on the nature of Ni and Cu deposits respectively. For Ni deposition shown in Table 4 6, semi-bright and dull/dark deposit were obtained below a duty cycle of 33.33%. Adherent, bright and shining deposits were obtained between duty cycle of 33 33% and 50% Above 60% duty cycle semi-bright deposits were obtained. These observations are explained in the following paragraph.

At constant frequencies, low duty cycles (< 33.33%), results in low pulse on-time and the effect of deposition is similar to that observed at high frequencies. For the bright and shining deposit (33 33%< DC< 50%) the low frequencies effect explanation given in the previous section holds good. However, at higher duty cycles (> 60%), an adherent and semi-bright nature of deposit is obtained. It can be explained that high duty cycle implies high pulse on-time, which increases the probability of H_2 evolution[1], a fact born by current efficiency (CE) measurements, as shown in Fig. 4 4 Fig. 4.4 shows that CE decreases from 85% to 58% as duty cycle increased from 40% to 80% In other experiment on Ni-Cu alloy deposition, Ghosh et. al. [40] also observed that with increasing duty cycle, the quality of deposit changes from very smooth, bright to non-metallic black and powdery. Powdery deposit implies mass transfer controlled deposition which was not observed in our case because of relatively high concentration Ni in the electrolyte. Ghosh and co-workers further observed that current efficiency of alloy deposition decreased as duty cycle was increased.

The effect of duty cycle on Copper deposition (as shown in Table 4.7) is not similar to that in case of Nickel. The major difference in the two cases is that bright deposits were obtained at duty cycle as high as 90%, which can be attributed of the absence of the H_2 evolution reaction ($E^0_{H^+/H2}$ = 0.0 V and $E^0_{Cu^{++}/Cu}$ = 0.34 V). Fig. 4 4 shows that CE of Cu deposition is almost constant (93%) from 20% to 90% duty cycle.

[1] The evolution of H_2 gas bubbles at the cathode could lead to porous structure.

Table 4 6 Effect of duty-cycle on the electro-deposition of Nickel at V_{Ni} = 2.95 V and pulse frequency 0 167 Hz

Duty Cycle (%)	Surface Appearance	No. of Cycles
10	No Ni deposition	30
20	Adherent, dull, dark	15
25	Adherent, semi-bright	12
33 33	Adherent, bright, shining	9
40	Adherent, bright, shining	7
50	Adherent, bright, shining	6
60	Adherent, semi-bright	5
70	Adherent, semi-bright	4
80	Adherent, semi-bright	4
90	Adherent, semi-bright	3

Table 4.7. Effect of duty-cycle on the electro-deposition of Copper at V_{Cu} = 1.245 V and pulse frequency 0.10 Hz.

Duty Cycle (%)	Surface Appearance	No. of Cycles
10	No Cu deposition	100
20	Adherent, semi-bright	50
30	Adherent, bright	33
40	Adherent, bright	25
50	Adherent, bright	20
60	Adherent, bright	16
70	Adherent, bright	14
80	Adherent, bright	12
90	Adherent, bright	11

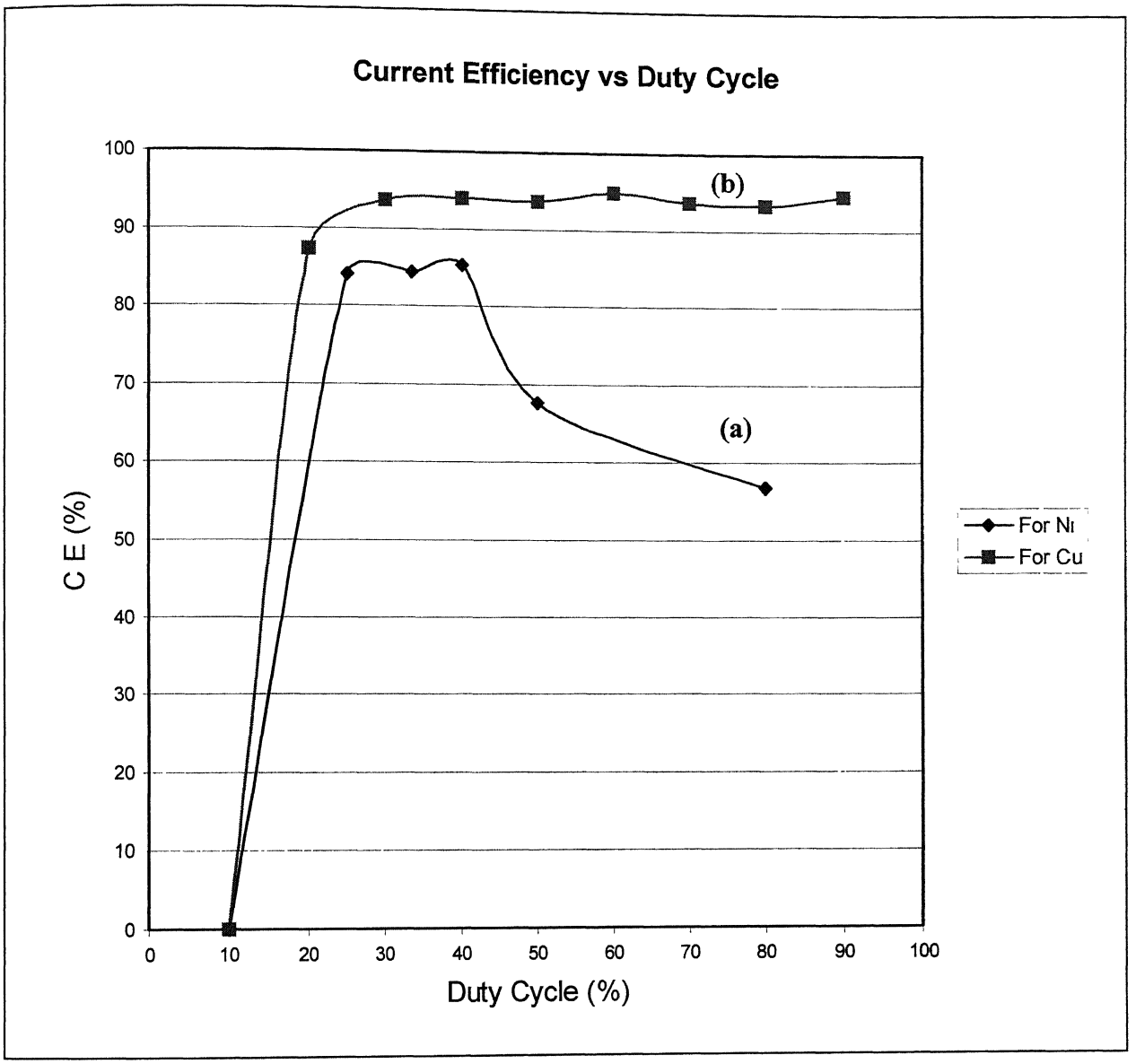

Figure 4.4. The effect of duty cycle on cathodic current efficiency for (a) Ni plating at V_{Ni} = 2.95 V and frequency of 0.167 Hz and (b) Cu plating at V_{Cu} = 1.245 V and frequency of 0.10 Hz

4.1.4. Effect of Number of Cycles

Tables 4 8 and 4.9 depict the effect of number of cycles on the nature of Ni and Cu deposits respectively

For Ni deposition, shown in Table 4 8, adherent, bright and shining deposits were obtained below of 35 cycles As the number of cycles increases above 35, the deposits becomes semi-bright and dull/dark

For Cu deposition as shown in Table 4 9, adherent and bright deposits were obtained below 60 cycles As the number of cycles increases above 60 the deposits becomes semi-bright.

Table 4 8 Effect of number of cycles on the electro-deposition of Nickel at V_{Ni} = 2.95 V, pulse frequency of 0 167 Hz and duty cycle of 33.33%

No. of Cycles	Surface Appearance
4	Adherent, bright, shining
10	Adherent, bright, shining
15	Adherent, bright, shining
20	Adherent, bright, shining
30	Adherent, bright
35	Adherent, bright
40	Adherent, semi-bright
45	Adherent, dull, dark
50	Adherent, dull, dark
60	Adherent, dark, dull

Table 4.9. Effect of number of cycles on the electro-deposition of Copper at V_{Cu} = 1.245 V, pulse frequency of 0.10 Hz and duty cycle of 90%. The pH of electrolyte is 2.10.

No. of Cycles	Surface Appearance
3	Adherent, bright
6	Adherent, bright
12	Adherent, bright
20	Adherent, bright
30	Adherent, bright
40	Adherent, bright
50	Adherent, bright
60	Adherent, bright
70	Adherent, semi-bright
90	Adherent, semi-bright

4.2. Effect of Bath Composition

4.2.1. Effect of $NiSO_4$ concentration

Tables 4.10 and 4.11 show the effect of $NiSO_4$ concentration on the nature and current efficiency of Ni and Cu deposits respectively

It is shown that the concentration of $NiSO_4$ does not affect the quality and current efficiency of Ni deposition (refer to Table 4 10). In all three concentrations, the deposits were adherent, bright and shining At concentration of 100 g/l the current efficiency is 82 66%, at 200 g/l it is about 84.41% and 84 74% at 280 g/l concentration So the results support the above statement In case of copper, deposits were adherent and bright in all three concentrations of $NiSO_4$ The current efficiencies are almost same at different concentration of $NiSO_4$ (Table 4 11)

The cathode current density for sound nickel deposits is a function of nickel ion concentration in the cathode film, which depends on the metal ion in the bath itself. A larger amount of nickel sulphate is used in the bath not only raises the limiting cathode current density but also lowers the resistivity of the electrolyte, thus improving current distribution.

Table 4 10. Effect of $NiSO_4$, $6H_2O$ concentration on the electro-deposition of Nickel at V_{Ni} = 3 V, frequency of 0 167 Hz, duty cycle of 40% and number of cycles are 15 Other constituent concentrations: $MgSO_4$, $7H_2O$ = 120 g/l, $CuSO_4$, $5H_2O$ = 2 g/l, H_3BO_3 = 30 g/l

$NiSO_4$ concentration (g/l)	**Surface Appearance**	**C.E (%)**
100	Adherent, bright	82 66
200	Adherent, bright, shining	84 41
280	Adherent, bright, shining	84.74

Table 4 11. Effect of $NiSO_4$, $6H_2O$ concentration on the electro-deposition of Copper at V_{Cu} = 1 245 V, frequency of 0.10 Hz, duty cycle of 90% and number of cycles are 15. Other constituent concentrations $MgSO_4$, $7H_2O$ = 120 g/l, $CuSO_4$, $5H_2O$ = 2 g/l, H_3BO_3 = 30 g/l.

$NiSO_4$ concentration (g/l)	**Surface Appearance**	**C.E (%)**
100	Adherent, bright	93 40
200	Adherent, bright	94.10
280	Adherent, bright	93.79

4.2.2. Effect of $MgSO_4$ concentration

Tables 4.12 and 4 13 depict the effect of $MgSO_4$ concentration on the nature and current efficiency of Ni and Cu deposits respectively.

For Ni deposition shown in Table 4 12, the concentration of $MgSO_4$ does not affect the quality and current efficiency of Ni deposition. In all four concentrations, the deposits were adherent, bright and shining. The current efficiency was about 85% in all four concentrations In case of copper, deposits were adherent and bright in all four concentrations of $MgSO_4$ The current efficiencies were almost same (about 94%) at these concentrations of $MgSO_4$ (Table 4 13)

The principle effect of $MgSO_4$ is to increase the conductivity of the electrolyte It was shown that as the concentration of $MgSO_4$ increases from 20 g/l to 160 g/l, the conductivity of the electrolyte increases 43 m mho/cm to 57.4 m mho/cm (Tables 4.12 and 4 13), hence the $I.R_{Solution}$ loss is minimized

Table 4.12. Effect of $MgSO_4$, $7H_2O$ concentration on the electro-deposition of Nickel at V_{Ni} = 3 V, frequency of 0 167 Hz, duty cycle of 40% and number of cycles are 15. Other constituent concentrations· $NiSO_4$, $6H_2O$ = 280 g/l, $CuSO_4$, $5H_2O$ = 2 g/l, H_3BO_3 = 30 g/l.

$MgSO_4$ concentration (g/l)	**Conductivity (m mho/cm)**	**Surface Appearance**	**C.E (%)**
20	43	Adherent, bright, shining	81 07
80	46 4	Adherent, bright, shining	85.57
120	52 6	Adherent, bright, shining	86.83
160	57 4	Adherent, bright, shining	88.64

Table 4.13. Effect of $MgSO_4$, $7H_2O$ concentration on the electro-deposition of Copper at V_{Cu} = 1.245 V, frequency of 0.10 Hz, duty cycle of 90% and number of cycles are 15. Other constituent concentrations $NiSO_4$, $6H_2O$ = 280 g/l, $CuSO_4$, $5H_2O$ = 2 g/l, H_3BO_3 = 30 g/l

$MgSO_4$ concentration (g/l)	**Conductivity (m mho/cm)**	**Surface Appearance**	**C.E (%)**
20	43	Adherent, bright,	94 37
80	46 4	Adherent, bright,	92 70
120	52.6	Adherent, bright,	94.69
160	57.4	Adherent, bright,	96.36

4.2.3. Effect of H_3BO_3 concentration

Tables 4.14 and 4 15 show the effect of H_3BO_3 concentration on the nature and current efficiency of Ni and Cu deposits respectively.

It is shown that the concentration of H_3BO_3 does not affect the current efficiency of Ni deposition (see Table 4 14) The current efficiencies were almost same (84 %) in all four concentrations of H_3BO_3. Even at the absence of H_3BO_3 the current efficiency is about 83 5%. But at low concentration of H_3BO_3 (up to 15 g/l), Ni deposits were adherent and semi-bright. But at higher concentrations (>15g/l) of H_3BO_3 the deposits were adherent, bright and shining.

For Cu deposition as shown in Table 4 15, adherent and bright deposits were obtained in all four concentration of H_3BO_3. The current efficiencies are almost same (93.5%) in all cases.

Boric acid serves as a week buffer in the plating solution. Its principle effect is that of controlling the pH of the electrolyte In the absence of buffer, nickel deposit at ordinary temperature tends to be hard, cracked and pitted. Furthermore, it produces whiter deposits, is helpful in its smoothing action on the deposit, and is unique in its cooperative effect with leveling addition agents.

Table 4 14. Effect of H_3BO_3 concentration on the electro-deposition of Nickel at V_{Ni} = 3 V, frequency of 0 167 Hz, duty cycle of 40% and number of cycles are 15. Other constituent concentrations. $NiSO_4$, $6H_2O$ = 280 g/l, $MgSO_4$, $7H_2O$ = 120 g/l $CuSO_4$, $5H_2O$ = 2 g/l

H_3BO_3 concentration (g/l)	**Surface Appearance**	**C.E (%)**
0	Adherent, semi-bright	83.52
5	Adherent, semi-bright	84 50
15	Adherent, bright	84 46
30	Adherent, bright, shining	84 33
45	Adherent, bright, shining	84.82

Table 4.15. Effect of H_3BO_3 concentration on the electro-deposition of Copper at V_{Cu} = 1.245 V, frequency of 0.10 Hz, duty cycle of 90% and number of cycles are 15. Other constituent concentrations: $NiSO_4$, $6H_2O$ = 280 g/l, $MgSO_4$, $7H_2O$ = 120 g/l, $CuSO_4$, $5H_2O$ = 2 g/l.

H_3BO_3 concentration (g/l)	**Surface Appearance**	**C.E (%)**
0	Adherent, bright	93.26
5	Adherent, bright	93.27
15	Adherent, bright	92.76
30	Adherent, bright	94.43
40	Adherent, bright	95 06

4.2.4. Effect of pH of electrolyte

Tables 4.16 and 4.17 depict the effect of pH on the nature and current efficiency of Ni and Cu deposits respectively

It was shown that in all the experiments the pH of the electrolyte affects only the cathodic current efficiency of nickel Because, H_2 evolution reaction ($E^0_{H^+/H2}$ = 0.0 V and $E^0_{Ni^{++}/Ni}$ = - 0 25V) takes place at the time of Ni deposition which reduce the current efficiency for Ni deposition. At very low pH (pH = 1 0) there was no Ni deposition as shown in Table 4.16, because the total current was utilized for H_2 evolution But in the pH range between 2 1 to 2.9, the deposits were bright, adherent and shining. This finding implied that the hydrogen evolution reaction at the cathode had been depressed when the pH value of the solution was relatively higher i e. the concentration of H^+ ion in the electrolyte is less. This causes zero current efficiency for nickel plating at pH = 1 but 84% between pH 2.1 to 2 9.

But there was almost no effect of pH of the electrolyte on the nature and current efficiency of copper plating. Bright and adherent deposits of Cu were obtained in three different pH of electrolyte. This is due to absence of the H_2 evolution reaction ($E^0_{H^+/H2}$ = 0.0 V and $E^0_{Cu^{++}/Cu}$ = 0.34 V), which implies the current efficiency for copper deposition is almost same (94%) in all three pH ranges as shown in Table 4.17.

Table 4 16. Effect of pH on the electro-deposition of Nickel at V_{Ni} = 3 V, frequency of 0 167 Hz, duty cycle of 40% and number of cycles are 15. Composition of Electrolyte: $NiSO_4$, $6H_2O$ = 280 g/l, $MgSO_4$, $7H_2O$ = 120 g/l $CuSO_4$, $5H_2O$ = 2 g/l and H_3BO_3 = 30 g/l

pH	Surface Appearance	C.E (%)
1.00	No Ni deposition	0
2 10	Adherent, bright, shining	83.46
2.90	Adherent, bright, shining	83.89

Table 4.17. Effect of pH on the electro-deposition of Copper at V_{Cu} = 1 245 V, frequency of 0.10 Hz, duty cycle of 90% and number of cycles are 15 Composition of Electrolyte: $NiSO_4$, $6H_2O$ = 280 g/l, $MgSO_4$, $7H_2O$ = 120 g/l $CuSO_4$, $5H_2O$ = 2 g/l and H_3BO_3 = 30 g/l.

pH	Surface Appearance	C.E (%)
1.00	Adherent, bright	93.23
2.10	Adherent, bright	93.87
2 90	Adherent, bright	93 78

Table 4.19. The different multilayered structure of Cu and Ni with different number of sub-layers

Exp No.	V_{Ni}/V_{Cu} (V)	Peak Current (A)	Frequency (Hz)	Duty Cycle (%)	Surface Appearance	No of Cycle	Total No. of Layer	Sub Layer Thickness (nm)
1.								
For Ni	2.84	0.54	0.167	33.33	Adherent, Bright,	15	3	300
For Cu	1.114	0.007	0.08	80	shining	15	3	60
2.								
For Ni	2.84	0.54	0.167	33.33	Adherent, Bright,	15	7	407
For Cu	1.367	0.01	0.08	80	shining	15	7	60
3.								
For Ni	2.91	0.56	0.167	33.33	Adherent, Bright,	15	10	420
For Cu	1.245	0.008	0.08	90	shining	15	10	52
4.								
For Ni	3.12	0.64	0.167	33.33	Adherent, Bright,	5	20	162
For Cu	1.369	0.01	0.08	90	shining	5	20	16

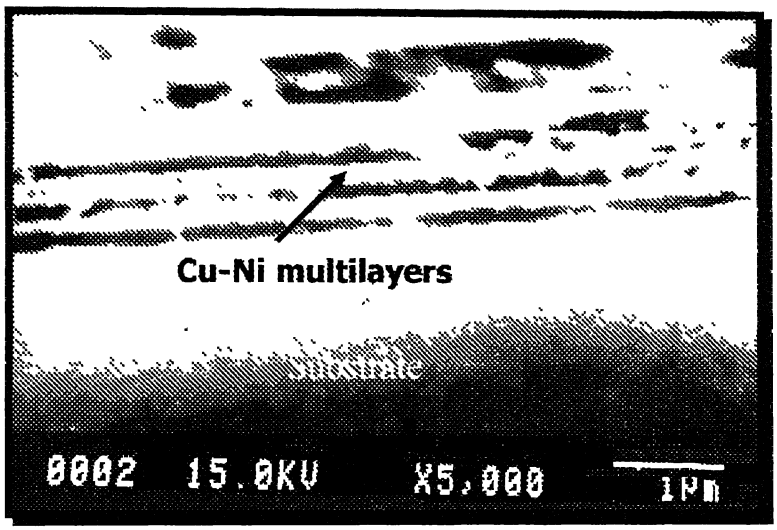

Figure 4 5. The EPMA micrograph of a etched (done by the solution containing 1 g $K_2Cr_2O_7$, 2 ml H_2SO_4 and 0 1 ml HCl) multilayer (6 layers) copper-nickel CMA alloy showing layers are not uniform for large distances. 300 nm nickel sub-layer, 60 nm copper sub-layer (Sample was taken from Exp. No 1, Table 4.19). The layers are adhering with the copper substrate. White lines are Ni layers and Black lines are Cu layers.

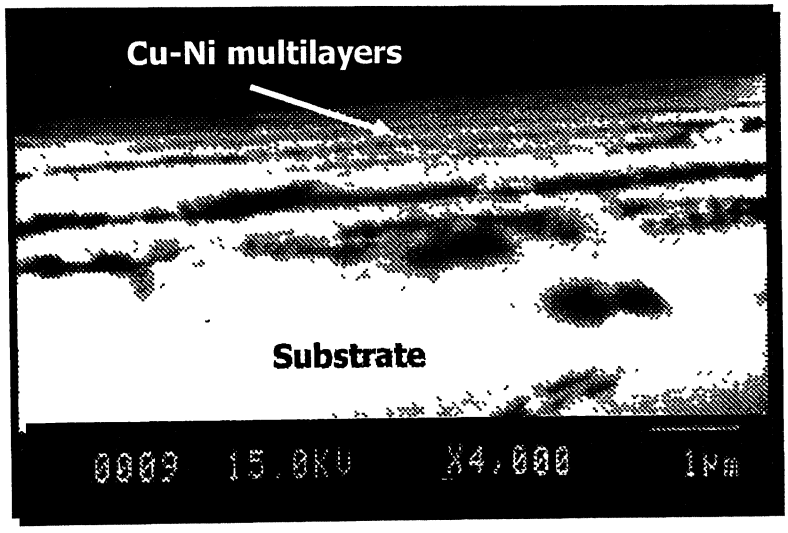

Figure 4.6 The EPMA micrograph of a etched (done by the solution containing 1 g $K_2Cr_2O_7$, 2 ml H_2SO_4 and 0 1ml HCl) multilayer (14 layers) copper-nickel CMA alloy showing layers uniformly for large distances. 407 nm nickel sub-layer, 60 nm copper sub-layer (Sample was taken from Exp. No. 2, Table 4.19). The layers are adhering with the copper substrate White lines are Ni layers and Black lines are Cu layers.

4.4.1. X-Ray Diffraction Analysis

The X-ray diffraction spectra for two Cu-Ni multilayers are shown in Fig. 4.7 and 4 8. The X-ray diffraction patterns of Cu-Ni multilayers display a mixed [111], [200], [220] and [311] texture But the peak intensity from the [111] plane of copper and nickel are much greater with respect to the standard values intensities from [200], [220] and [311] planes This indicates the electrodeposited multilayered Cu & Ni have a pronounced [111] texture. The diffraction spectrum also shows that the layers composed of only Ni and Cu This indicates that there was no alloying of Ni and Cu at the interface

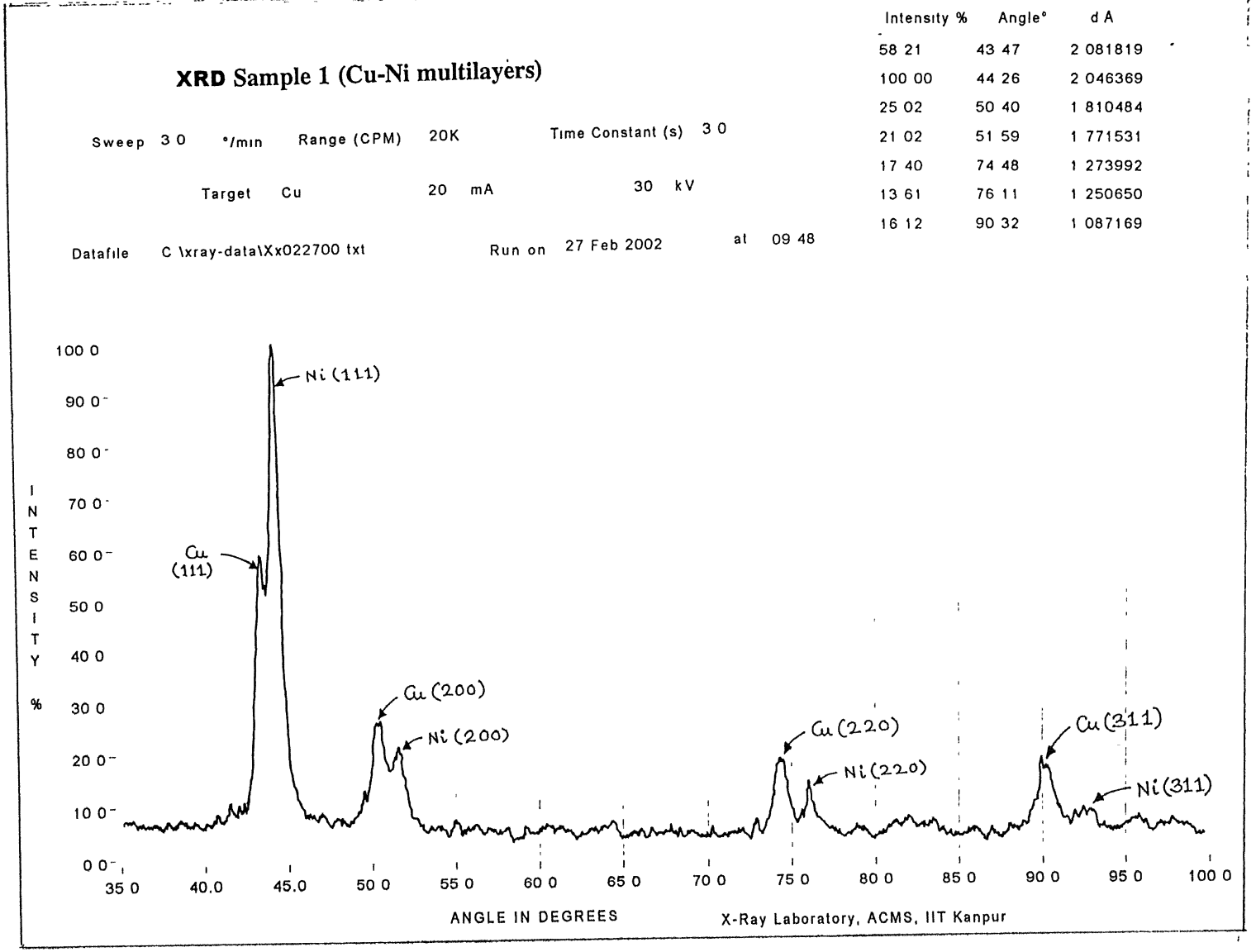

Fig. 4.7. X-RD spectrum for Cu-Ni multilayers. The Cu-Ni multilayers consist of three layers each of Ni and Cu; the individuallayer thickness being 300 nm and 60 nm respectively.

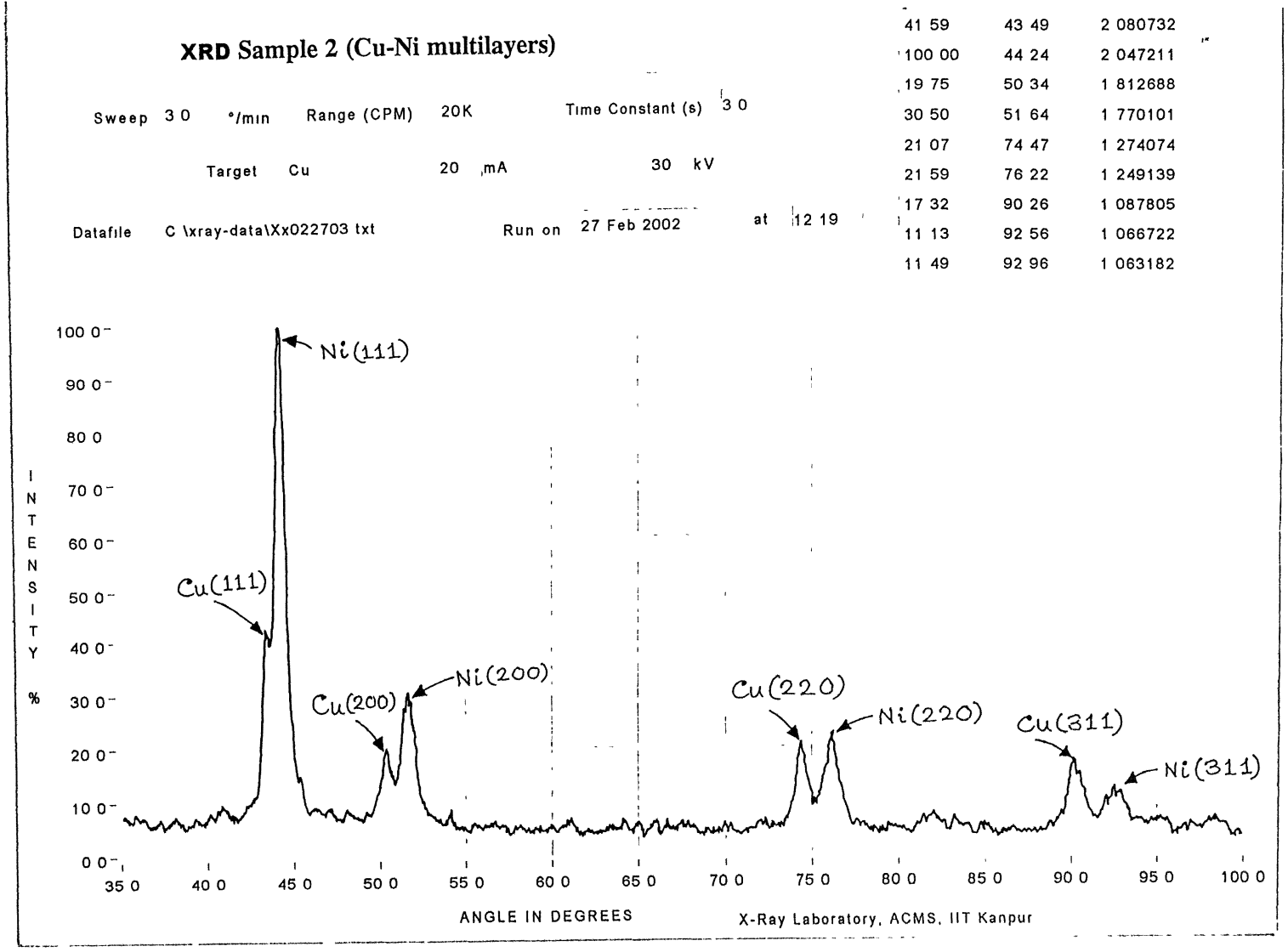

Fig. 4.8. X-RD spectrum for Cu-Ni multilayers. The Cu-Ni multilayers consist of seven layers each of Ni and Cu; the individual layer thickness being 407 nm and 60 nm respectively.

4.4.2. Magnetic Characterization

The temperature dependence of the magnetisation of Cu-Ni multilayers in an applied field of 1260 Oe are shown for successive heating and cooling run for sample in Fig 4 9 - 10. A lowering of magnetic moment in the cooling run was noticed. For both two samples the Curie point of Ni (T_C = 360^{0}C) is detected in our measurements In the cooling run the magnetic moment decreases for any temperature w.r.t. heating run. This is due to diffusion of Ni and Cu at the interface, which destroyed the multilayered structure and produced a uniform layer consisting of Cu-Ni solid solution

The thermal stability of compositionally modulated multilayers (CMM) is an important limitation towards their application. In the case of CMMs consisting of an alternation of magnetic and non-magnetic sublayers, magnetic properties are altered by diffusion between the sublayers. A method for studying the diffusion in magnetic CMMs, based on the decrease in magnetisation with time and temperature, was developed for two Cu–Ni CMMs with a sublayer thickness of Ni is 300 nm and Cu is 60 nm (sample 1) and Ni is 407 nm and Cu is 60 nm (Sample 2) The total thicknesses are of 1080 nm (Sample 1) and 3269 nm. In order to demonstrate the suitability, the magnetisation at room temperature (25^{0}C) was measured as a function of diffusion time at a constant temperature for a Cu–Ni CMM samples with different sublayer (Sample 1 of 6 layers and Sample 2 of 14 layers) thicknesses. The time of diffusion was added up for each successive step of heating and the corresponding magnetic moments were recorded The results are shown in Fig. 4.11

The results confirm that diffusion through a planar layer follows the parabolic law [41] According to the model [41], the following equations describe the diffusion process.

$$\frac{M}{W} = A - B\sqrt{t} \quad \ldots\ldots\ldots\ldots (1)$$

$$B = A\left(\frac{N}{L}\right)\sqrt{D} \quad \ldots\ldots\ldots (2)$$

$$A = m_{Ni}/(1+F)$$

Where, M = total magnetic moment, W = total mass of the sample, m_{Ni} = magnetic moment per unit mass of Ni, F = ratio of atomic weights of Ni and Cu, N = number of sublayers, L = total thickness and D = diffusion coefficient. The parameters A and B are determined by a linear fit of the experimental data as plotted in Fig 4.9.

If D follows an Arrhenius law $D = D_0 \exp -(Q/RT)$, the activation energy Q associated with diffusion process and can easily calculated from the equation:

$$\frac{d(\log B)}{d(1/T)} = -\frac{Q}{2R} \quad \ldots\ldots\ldots\ldots\ldots\ldots (3)$$

Where, R is the gas constant, Q can be determined from the slope of the plot $log\ B$ versus $1/T$

Table 4.20. Slope, B, and intercept, A, of the linear fit of the experimental data in Fig. 4.9 - 10 for two Cu–Ni CMM multilayers with different thicknesses.

Sample	L (nm)	N	B (emu. $g^{-1}.s^{-1/2}$)	A (emu. g^{-1})
(Ni 300 nm/Cu 60 nm) x 3	1080	6	0.384	134.7368
(Ni 407 nm/Cu 60 nm) x 7	3269	14	0.118	53.7696

Table 4.20 shows the parameters $B1$, $B2$, $A1$ and $A2$ of the two samples. To confirm the validity of Equation (2), we can compare the ratio $[(B1/A1)/(B2/A2)]$ with $[(N1/L1)/(N2/L2)]$, the result of which gives an error of 1%.

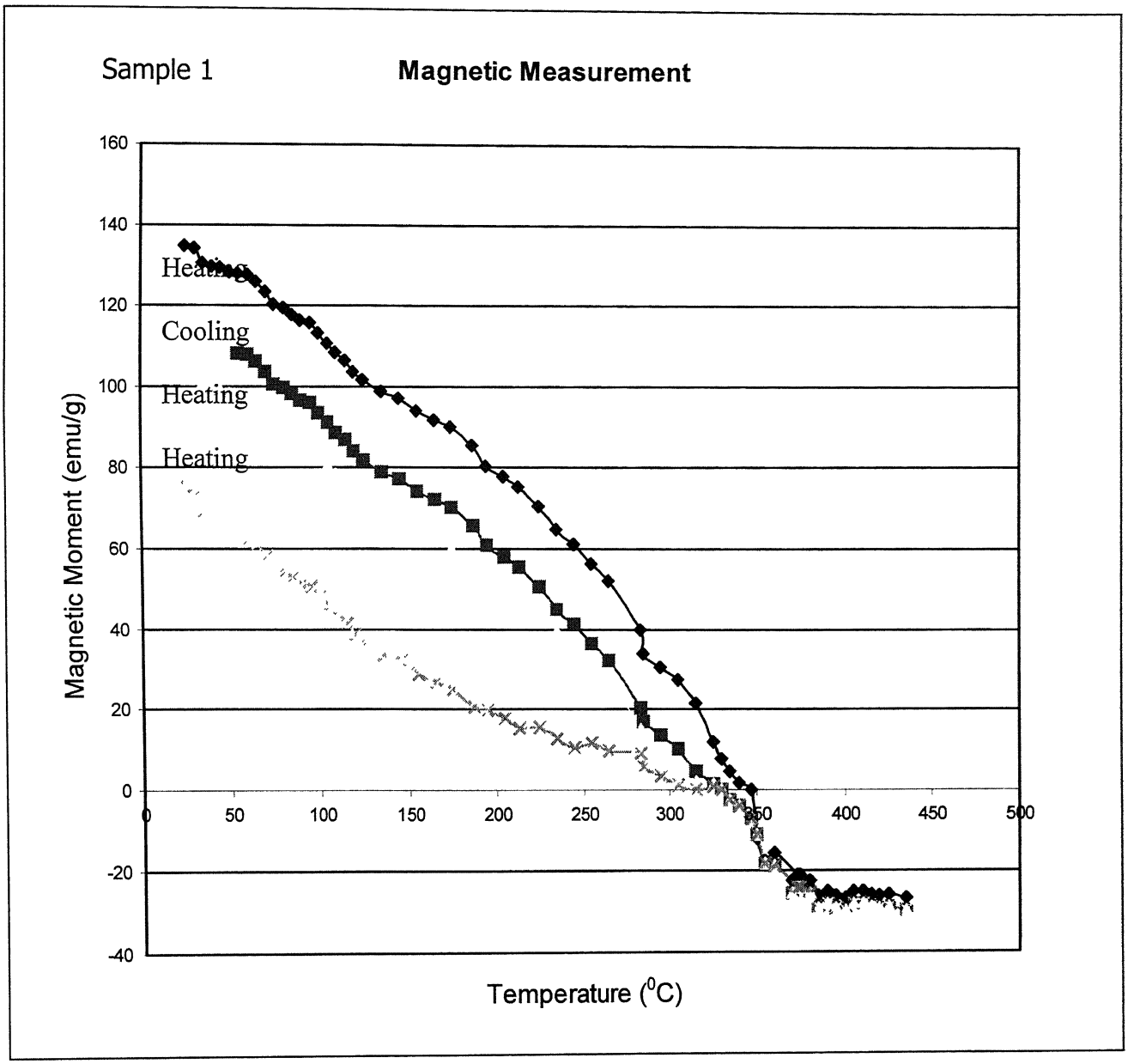

Figure 4.9. Magnetization of Cu-Ni multilayer as a function of temperature for several consecutive runs. The Cu-Ni multilayers consist of three layers each of Ni and Cu; the individual layer thickness being 300 nm and 60 nm respectively.

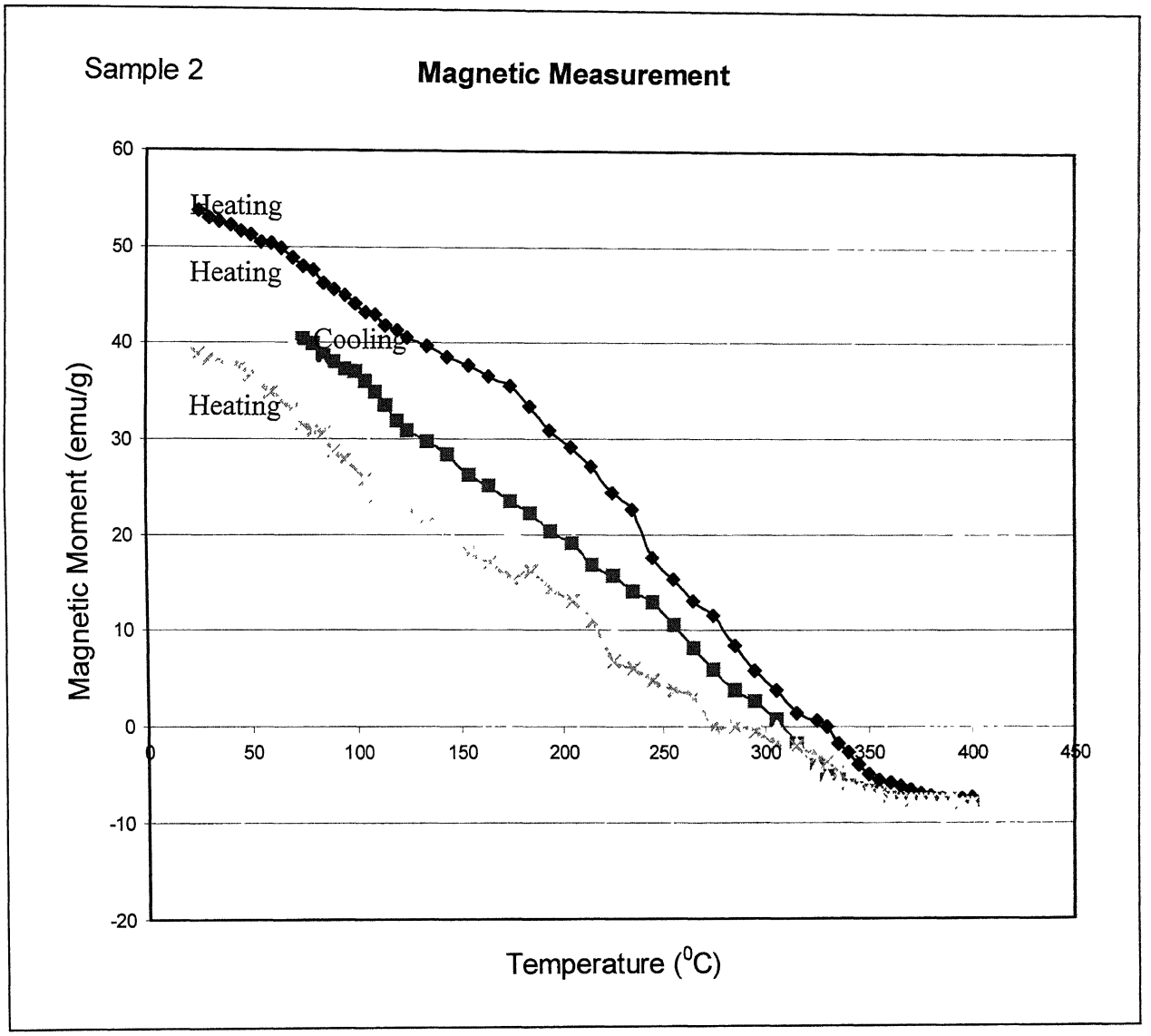

Figure 4.10. Magnetization of Cu-Ni multilayer as a function of temperature for several consecutive runs. The Cu-Ni multilayers consist of seven layers each of Ni and Cu; the individual layer thickness being 407 nm and 60 nm respectively.

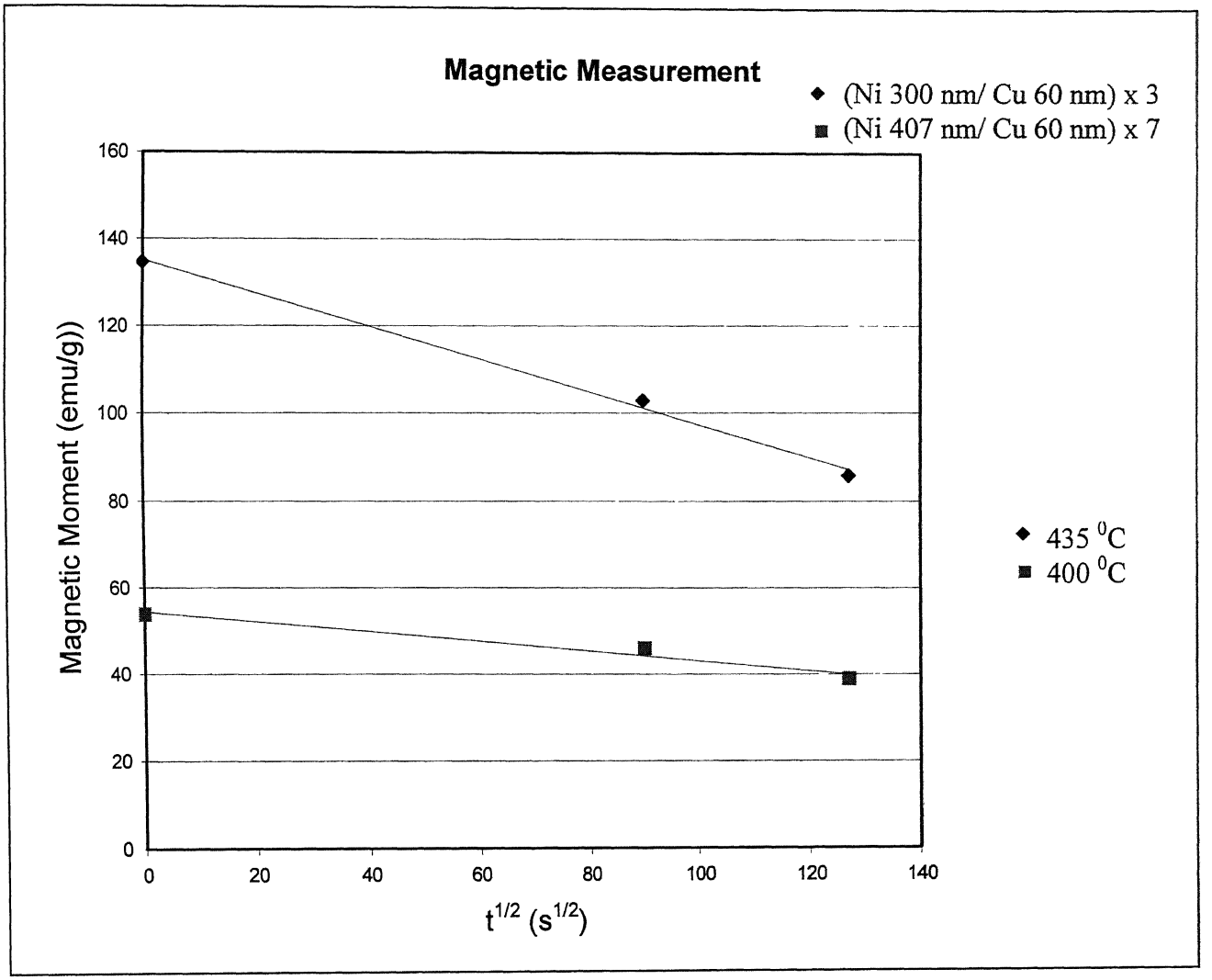

Figure 4.11. Magnetic moment per unit mass at room temperature of a Cu–Ni multilayer at an applied field H = 1260 Oe, as a function of the square root of the diffusion time. Diffusion took place at T = 435 °C and T = 400 °C.

CHAPTER V

SUMMARY AND CONCLUDING REMARKS

Compositionally modulated multilayers (CMM) consisting of alternate layers of magnetic and non-magnetic alloys exhibit Giant Magneto-Resistance. This means that if their resistance is monitored, materials exhibiting GMR can be used to detect magnetic fields CMM have been produced by vacuum evaporation techniques. Production of multilayers by electrodeposition has a number of advantages over vacuum techniques such as low cost process, simple equipment, higher (5 μm/min) deposition rate, precise deposition control and low interdiffusion between sub-layers due to lower deposition temperature

Electrodeposition of Cu-Ni multilayer was carried out from a single bath using pulse voltage The main objective of this research has been to optimize pulse parameters (applied voltage, frequency, duty cycle and number of cycle) and electrolyte composition for deposition of Cu, Ni and Cu-Ni multilayers The deposit was characterized by (i) visual appearance, that is, whether it was dull/dark or bright or shining and (ii) adherence to the substrate. After determination of the effect of pulse parameters, electrolyte composition and pH on the quality of Cu and Ni electrodeposit, the best operating conditions were determined as follows-

	For Cu plating	**For Ni plating**
Voltage:	1 062V - 1.498V	2.91V - 3.287V
Frequency:	1.25 Hz - 0.025 Hz	1.67 Hz - 0.069 Hz
Duty Cycle:	70 % - 90 %	33.33 % – 50 %
No. of Cycle:	3 – 60	5 – 35
H_3BO_3 Conc.:	30 g/l – 45 g/l	30 g/l – 45 g/l
pH:	2 10 – 2.90	2.10 – 2.90

CHAPTER VI

RECOMMENDATION FOR FUTURE WORKS

The following features can be added in future:

1. Extensive microstructural characterization of multilayer electrodeposit of Cu-Ni multilayer.
2. Galvanostatic deposition of Cu-Ni multilayer and their characterization.
3. Development of mathematical models for optimization of process parameters.

APPENDIX-I

Voltage calculation for Ni and Cu Electrodeposition

Conductivity of the solution = 52 6 m mho/cm

(For bath composition: $NiSO_4$ = 280 g/l, $CuSO_4$ = 2 g/l, H_3BO_3 = 30 g/l, $MgSO_4$ = 120 g/l)

Inter Electrode Distance (L) = 2 cm

For Copper deposition:

Required current density (i_{Cu}) < 10 A/m^2

Reactions

At anode: $2\ H_2O \leftrightarrows O_2 + 4\ H^+ + 4e$	$E^0_a = -1.27$ V
At cathode: $Cu^{++} + 2e \leftrightarrows Cu$	$E^0_c = +0.34$ V
$Cu^{++} + 2\ H_2O \leftrightarrows Cu + O_2 + 4\ H^+$	$E^0_{Cell} = -0.93$ V

Applied potential (**V**) = $|E_{Cell}| + I\ R_{Solution}$ (omitting other overpotentials)

$= |E_{Cell}| + I\ (\rho.\ L/A)$

$= |E_{Cell}| + i.\rho.\ L$ ----------(1)

Where,

E_{Cell} = Standard Cell potential for nickel and copper deposition

I = the current passing through the cell.

i = the current density at electrodes = I/**A**

ρ = Resistivity of the Electrolyte = 1/Conductivity

L = Distance between the electrodes.

A = Area of deposition = 22.5 cm^2

Putting, E_{Cell} = -0.93 V, i = 0.001 A/cm^2, ρ = 1/52.6 m mho^{-1}.cm, L = 2 cm, in the Equation.1.

The calculated value of Applied potential (**V**) ≈ 1V

For Nickel deposition:

Required current density (i_{Ni}) ≥ 100 A/m^2

Reactions:

At anode: $2\,H_2O \leftrightarrows O_2 + 4\,H^+ + 4e$ $\quad E^0_a = -1.27$ V

At cathode: $Ni^{++} + 2e \leftrightarrows Ni$ $\quad E^0_c = -0\ 25$ V

$Ni^{++} + 2\,H_2O \leftrightarrows Ni + O_2 + 4\,H^+$ $\quad E^0_{Cell} = -1.52$ V

Putting, E_{Cell} = -1.52 V, i = 0.01 A/cm^2, ρ = 1/52.6 m mho^{-1}.cm, L = 2 cm, in the Equation.1.

The calculated value of Applied potential (**V**) ≈ 2 V

APPENDIX-II

Sub-layer Thickness Measurement

For Nickel Sub-layer Thickness:

The current efficiency (C.E) for Ni deposition = 84% (in the best condition)

Area of deposition (**A**) = 22.5 cm^2

Atomic weight of Ni = 58.6934

Density of Ni = 8.908 gm/c.c

Charge for deposition (Q) = I. T

[Where, I = deposition current (in Ampere)

T = deposition time (in second)]

Q = I x 1/Frequency (Hz) x Duty Cycle (%) x No. of Cycle (N) x C.E (%)

= I x (1/F) x (DC) x N x (CE)

Weight of Ni deposited (W) = (58.6934 x Q) / (2 x 96496) gm

Thickness of deposition (t) = W / (**A** x 8.908) cm

Thickness (t) = 15.1734 x I x (1/F) x (D.C) x N x (C.E) nm

For Copper Sub-layer Thickness:

The current efficiency (C.E) for Cu deposition = 94% (in the best conditions)

Area of deposition (**A**) = 22.5 cm^2

Atomic weight of Cu = 63.546

Density of Ni = 8.23 gm/c.c

Charge for deposition (Q) = I. T

[Where, I = deposition current (in Ampere)

T = deposition time (in second)]

Q = I x 1/Frequency (Hz) x Duty Cycle (%) x No. of Cycle (N) x C.E (%)

= I x (1/F) x (DC) x N x (CE)

Weight of Ni deposited (W) = (63.546 x Q) / (2 x 96496) gm

Thickness of deposition (t) = W / (A x 8.23) cm

Thickness (t) = 17.7814 x I x (1/F) x (D.C) x N x (C.E) nm

APPENDIX-III

"Head Start" Computer Programming for Electrodeposition

For Nickel Deposition:

```
DCL
FP 0
LP 120
MODE 2
MM 1
MR 2
I/E 0
AR 0
SCV 2
DCV 0
SIE 3
INTRP 0
TMB 10000
S/P 10
INITIAL 0 0
VERTEX 36 0
VERTEX 37 13000
VERTEX 59 13000
VERTEX 60 0
VERTEX 96 0
VERTEX 97 13000
VERTEX 119 13000
VERTEX 120 0
SWPS 15
ASM
NC
CELL 1
TC
g 0
CELL 0
```

The program gives:

Peak Voltage = 2.95 V

Peak Current = 0.62 A

Duty Cycle = 40 %

Frequency = 0.167 Hz

No. of Cycle = 15

For Copper Deposition:

DCL
FP 0
LP 200
MODE 2
MM 1
MR 2
I/E 0
AR 0
SCV 2
DCV 0
SIE 3
INTRP 0
TMB 10000
S/P 10
INITIAL 0 0
VERTEX 10 0
VERTEX 11 5000
VERTEX 99 5000
VERTEX 100 0
VERTEX 110 0
VERTEX 111 5000
VERTEX 199 5000
VERTEX 200 0
SWPS 15
ASM
NC
CELL 1
TC
g 0
CELL 0

The program gives:

Peak Voltage = 1.25 V

Peak Current = 0.01 A

Duty Cycle = 90 %

Frequency = 0.10 Hz

No. of Cycle = 15

APPENDIX-IV

Grain size measurement from X-Ray diffraction spectrum:

The grain size of the films was estimated using the Scherrer formula-

$$t = \frac{0.9\lambda}{BCos\theta_B} \quad \text{.....(1)}$$

Where,

t = grain diameter, in meter

λ = wavelength of monochromatic X-ray beam, in meter

B = full width at the half maximum of the peak, in radian

θ_B = Bragg angle, in degree

θ_B was calculated from the Bragg's law-

$$\lambda = 2d \text{ Sin } \theta_B$$

[d = lattice parameter, in meter]

Measurement of B:

The measurement of B is done by taking half of the distance between two extreme angles at which the intensity is zero, which amounts to assuming that the diffraction line is triangular in shape.

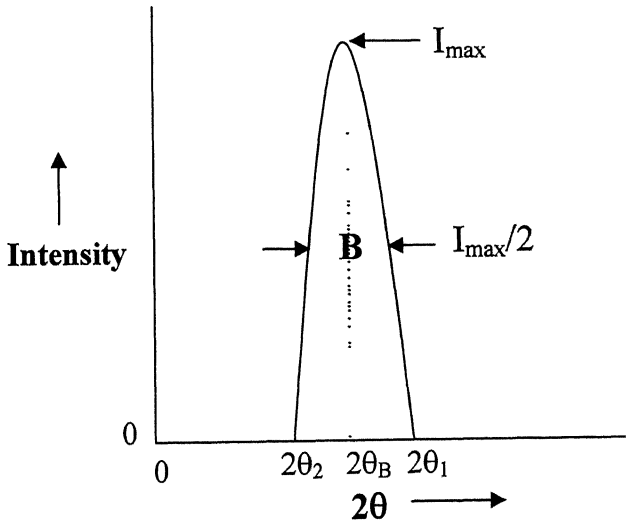

$$B = \tfrac{1}{2}(2\theta_1 - 2\theta_2) = (\theta_1 - \theta_2), \text{ in radians}$$

Grain size of Nickel deposition:

$\lambda = 1.54056$ Å

$d = 1.62$ Å

$\theta_B = \text{Sin}^{-1}(\lambda/2d) = 0.4955$

$$t = \frac{0.9X1.54056}{BCos\theta_B}\,^{0}A$$

$$\boxed{t = \frac{1.576064}{B}\,^{0}A}$$

Grain size of Copper deposition:

$\lambda = 1.54056$ Å

$d = 1.57$ Å

$\theta_B = \text{Sin}^{-1}(\lambda/2d) = 0.512806$

$$t = \frac{0.9X1.54056}{BCos\theta_B}\,^{0}A$$

$$\boxed{t = \frac{1.591175}{B}\,^{0}A}$$

REFERENCES

1. P. Grünberg, R. Schreiber, Y. Pang, M. B. Brodsky, and H. Sowers, "Layered Magnetic Structures: Evidence for Antiferromagnetic Coupling of Fe Layers Across Cr Interlayers," *Phys. Rev. Lett.* 57, No. 19, 2442 (1986).

2. C.H.Smith, R.W.Schneider, "The Growing Role of Solid-State Magnetic Sensing" Proceedings Sensors Expo Boston, pp. 139-149 (Helmers, Peterborough, NH,1997).

3. M. N. Baibich, J. M. Broto, A. Fert, F. Nguyen Van Dau, F. Petroff, P. Etienne, G. Creuzet, A. Friederich, and J. Chazelas, "Giant Magnetoresistance of (001)Fe/(001)Cr Magnetic Superlattices," *Phys. Rev. Lett.* 61, 2472-2475 (1988).

4. G. Binasch, P. Grünberg, F. Saurenbach, and W. Zinn, "Enhanced Magnetoresistance in Layered Magnetic Structures with Antiferromagnetic Interlayer Exchange," *Phys. Rev. B* 39, 4828-4830 (1989).

5. S. S. P. Parkin, N. More, and K. P. Roche, "Oscillations in Exchange Coupling and Magnetoresistance in Metallic Superlattice Structures: Co/Ru, Co/Cr, and Fe/Cr," *Phys. Rev. Lett.* 64, 2304-2307 (1990).

6. S. S. P. Parkin, "Systematic Variation of Strength and Oscillation Period of Indirect Magnetic Exchange Coupling Through the 3d, 4d and 5d Transition Metals," *Phys. Rev. Lett.* 67, 3598 (1991).

7. S. S. P. Parkin, *IBM J. Res. Dev.*, 42(1) (1998).

8. J. M. Brownlow, " Electrodeposition of thin magnetic films in the Ni-Fe-Cu system," *J Appl. Phys., 38* (1967) 1440.

9. R. D. McMichael, U. Atzmony, C. Beauchamp, L. H. Bennett, L. J. Swartzendruber, D. S. Lashmore and L. T. Romankiw, " Fourfold anisotropy of an electrodeposited Co/Cu compositionally modulated alloys," *J. Magn. Magn. Mater., 113* (1992) 149-154.

10. M. Alper, P. S. Aplin, K. Attenborough, D. J. Dingly, R. Hart, S. J. Lane, D. S. Lasmore and W. schwarzacher, " Growth and characterization of electrodeposited Cu/Cu-Ni-Co alloys super lattice", *J. Magn. Magn. Mater., 126* (1993) 8-11.

11. D. Tench and J. White, " Enhanced tensile strength for electrodeposited nickel-copper multilayer composites," *Metall. Trans., 15A* (1984) 2039-40.

12. R. Weil, C. C. Nee and J. W. Chang, " Pulsed electrodeposition of layered brass structure," *Metall. Trans., 19A* (1988) 1569-73.

13. D. M. Tench and J. D. White, " Tensile properties of nanostructural Ni-Cu multilayered materials prepared by electrodeposition," *J. Electrochem. Soc., 138* (1991) 3757-3758.

14. A. W. Ruff and D. S. Lassmore, " Sliding wear studies of Ni-Cu composition-modulated coatings on steel," *Wear, 131* (1989) 259-272.

15. U. Cohen, F. B. Koch and R. Sard, " Electroplating of cyclic multilayered alloys (CMA) coatings," *J. Electrochem. Soc., 130* (1983) 1987-95.

16. J. DuMond and J. P. Youtz, " An X-ray method of determining rates of diffusion in the solid state," *J. Appl. Phys., 11* (1940) 357-365.

17. W. Blum, " The structure and properties of alternately electrodeposited metals," *Trans. Am. Electrochem. Soc , 40* (1921) 307-320.

18. P.Leisner, C. B. Nielsen, P. T. Tang, T. C. Dörge and P. Møller, " Methods for electrodepositing composition-modulated alloys," *Journal of Materials Processing Tech. 58* (1996) 39-44.

19. L. M. Goldman, B. Blanpain and F. Spaepen, " Short wavelength compositionally modulated Ni/Ni-P films prepared by electrodeposition," *J. Appl. Phys.,60* (1986) 1374-76.

20. L. M. Goldman, C. A. Ross, W. Ohashi, D. Wu and F. Spaepen, " New dual-bath technique for electrodeposition of short repeat length multilayers," *Appl. Phys. Lett., 55* (1989) 2182-84.

21. C. A. Ross, L. M. Goldman, W. Ohashi and F. Spaepen, " An electrodeposition technique for producing multilayers of nickel-phosphorous and other alloys," *J. Electrochem. Soc , 140* (1993) 91-98.

22. D. S. Lashmore and M. P. Dariel, " Electrodeposited Cu-Ni textured superlattices," *J. Electrochem. Soc., 135* (1988) 1218-21.

23. R. K. Nesbet, *IBM J. Res. Dev.,* 42(1) (1998).

24. S. S. P. Parkin, R. Bhadra, and K. P. Roche, *Phys. Rev. Lett.* 66, 2152 (1991).

25. G. A. Prinz and J. J. Krebs, *Appl. Phys. Lett.*, 39, 397 (1981).

26. P. Etienne, G. Creuzet, A. Friederich, F. Nguyen Van Dau, A. Fert, and J. Massies, *Appl Phys. Lett.*, 53, 162 (1988).

27. P. Leisner, C. B. Nielsen, P. T. Tang, T. C. Dorge and P. Moller, *J. Mat. Proc. Tech*, 58, 39 (1996).

28. S. K. J. Lenczowski, C. Schonenberger, M. A. M. Gijs and W. J. M. de Jonghe, *J. Magn. Magn. Mater.*, 148(3), 455 (1995).

29. Y. Jyoko, S. Kashiwabara and Y. Hayashi, *J. Electrochem. Soc.*, 144(7), L193 (1997).

30. Ch Bonhote and D. Landolt, *Electrochimica Acta*, 42(15), 2407 (1997).

31. W. Schwarzacher, M. Alper, R. Hart, G. Nabiyouni, I. Bakonyi and E. Toth-Kadar, *Electrochemical Synthesis and Modification*, Symposium proceedings, 451, Materials research Society, Pittsburgh, USA, 347 (1997).

32. A. Cziraki, I. Gerocs, B. Fogarassy, B. Arnold, M. Reibold, K. Wetzig, E. Toth-Kadar and I. Bakonyi, *Z Metallkd.*, 88, 781 (1997).

33. Y. Jyoko, S. Kashiwabara, Y. Hayashi : Preparation of Giant Magnetoresistance Cu-Co Heterogeneous Alloys by Electrodeposition, *J. Eletrochem. Soc.*, 144 (1997) 193-195.

34. E. To´th-Ka´da´r, L. Pe´ter, T. Becsei, J. To´th, L. Poga´ny, T. Tarno´czi, P. Kamasa, I. Bakonyi, G. La´ng, A´ . Czira´ki, and W. Schwarzacher, *J. Electrochem. Soc*, 147, 3311 (2000).

35. M. Alper, W. Schwarzacher and S. J. Lane, *J. Electrochem. Soc.*, 144, 2346 (1997).

36. L. Pe´ter, A. Czira´ki, L. Poga´ny, Z. Kupay, I. Bakonyi, M. Uhlemann, M. Herrich, B. Arnold, T. Bauer and K. Wetzig, *J. Electrochem. Soc.*, 148, C168 (2001).

37. Kasyutich O.I., W. Schwarzacher, V.M. Vedosyuk, P.A. Laskarzhevsky, A.I. Masliy, " Comparison of structure and magnetotransport properties of Co-Ni-Cu/Cu multilayers electrodeposited on (001) and (111) n-GaAs", *J. Electrochem. Soc.*, 2000, v.147, N8, p.2964-2968.

38. V. A. Zabludovsky and V. S. Gribok, " Physical properties of Ni-Cu mycrolayer films obtained by Pulse Electrolysis." *Trans. IMF 77(2)* (1999) 89-90.

39. S. E. Hadian and D. R. Gabe, " Control of Electrodeposit Properties of Nickel and Nickel-Iron Alloys by Pulse Plating", Metal Finishing.

40. S.K. Ghosh, A.K. Grover, G.K. Dey and M.K. Totlani, "Nanocrystalline Ni-Cu alloy plating by pulse electrolysis", *Surface and Coatings Technology, vol. 126 (2000),pp. 48-63.*

41. J. B. Oliveira, M.A. Sa, J.M. machado da Silva, G. Wouters and J. P. Celis, " Determination of diffusion in electrodeposited Cu-Ni compositionally-modulated multilayers based on magnetic measurement", *Journal of alloys and Compounds, 239 (1996) 41-45.*